

The CLIP-170 Homologue Bik1p Promotes the Phosphorylation and Asymmetric Localization of Kar9p[□]

Jeffrey K. Moore, Sonia D'Silva, and Rita K. Miller

Department of Biology, University of Rochester, Rochester, NY 14627

Submitted June 27, 2005; Revised October 5, 2005; Accepted October 12, 2005

Monitoring Editor: Tim Stearns

Accurate positioning of the mitotic spindle in *Saccharomyces cerevisiae* is coordinated with the asymmetry of the two poles and requires the microtubule-to-actin linker Kar9p. The asymmetric localization of Kar9p to one spindle pole body (SPB) and microtubule (MT) plus ends requires Cdc28p. Here, we show that the CLIP-170 homologue Bik1p binds directly to Kar9p. In the absence of Bik1p, Kar9p localization is not restricted to the daughter-bound SPB, but it is instead found on both SPBs. Kar9p is hypophosphorylated in *bik1Δ* mutants, and Bik1p binds to both phosphorylated and unphosphorylated isoforms of Kar9p. Furthermore, the two-hybrid interaction between full-length *KAR9* and the cyclin *CLB5* requires *BIK1*. The binding site of Clb5p on Kar9p maps to a short region within the basic domain of Kar9p that contains a conserved phosphorylation site, serine 496. Consistent with this, Kar9p is found on both SPBs in *clb5Δ* mutants at a frequency comparable with that seen in *kar9-S496A* strains. Together, these data suggest that Bik1p promotes the phosphorylation of Kar9p on serine 496, which affects its asymmetric localization to one SPB and associated cytoplasmic MTs. These findings provide further insight into a mechanism for directing centrosomal inheritance.

INTRODUCTION

Positioning of the mitotic spindle is critical for cell division in all eukaryotes. In the budding yeast *Saccharomyces cerevisiae*, the mitotic spindle is positioned across the plane of cytokinesis located at the mother-bud neck, yielding an asymmetric cell division. This requires both actin cables and cytoplasmic microtubules (cMTs) (Theesfeld *et al.*, 1999; Sullivan and Huffaker, 1992). The minus ends of cMTs emanate from a centrosome-like structure called the spindle pole body (SPB) embedded in the nuclear envelope (Byers and Goetsch, 1975).

Spindle positioning in yeast is governed by two sequential processes, termed the Kar9p pathway and the dynein pathway (Miller and Rose, 1998). Proteins in the Kar9p pathway function to move the nucleus up to the bud neck and align the mitotic spindle along the mother-bud axis before anaphase (DeZwaan *et al.*, 1997; Miller and Rose, 1998). In this process, cMTs are oriented toward both the bud neck and growing bud (Segal *et al.* 2000a; Kusch *et al.*, 2002). This involves a molecular bridge between actin and cMTs consisting of the type V myosin Myo2p, Kar9p, and the MT binding protein Bim1p (Beach *et al.*, 2000; Korinek *et al.*, 2000; Lee *et al.*, 2000; Miller *et al.*, 2000; Yin *et al.*, 2000; Hwang *et al.*, 2003). The kinesin Kip3p and the XMAP215/

TOG1 homologue Stu2p also contribute to the Kar9p pathway (DeZwaan *et al.*, 1997; Miller *et al.*, 1998; Kosco *et al.*, 2001). Together with the dynactin complex, dynein (*DYN1/DHC1*) and Num1p at the cortex exert pulling and sliding forces on cMTs (Muhua *et al.*, 1994; Adames and Cooper, 2000; Heil-Chapdelaine *et al.*, 2000; Yeh *et al.*, 2000; Farkasovsky and Kuntzel, 2001; Lee *et al.*, 2003). This moves the spindle across the plane of cytokinesis at (Yeh *et al.*, 1995) or just after (Kahana *et al.*, 1995) the onset of anaphase. The CLIP-170 homologue Bik1p and the kinesin Kip2p also function in the dynein pathway (Miller *et al.*, 1998; Miller and Rose, 1998).

The two pathways were initially defined by genetic analysis and are partially redundant (Miller and Rose, 1998). Double mutations within the same pathway are no more deleterious than either single mutation alone (Muhua *et al.*, 1994). However, simultaneous mutations between components of each pathway result in cell death, or synthetic lethality (Miller and Rose, 1998; Heil-Chapdelaine *et al.*, 2000). Although the kinesin Kip2p is genetically required for the dynein pathway, recent work has revealed a function for Kip2p in the Kar9p mechanism (Miller *et al.*, 1998; Maekawa *et al.*, 2003). This raises the question of how proteins may have functions in both pathways but seem genetically to be essential in only one.

The orientation of the mitotic spindle across the bud neck is coordinated with differences between the two SPBs. The old SPB is translocated into the bud and the new SPB is retained in the mother cell (Pereira *et al.*, 2001). During G₁, Kar9p localizes to the unduplicated SPB (Maekawa *et al.*, 2003). After SPB duplication, Kar9p remains associated with the older SPB. This asymmetric restriction involves the cell cycle-dependent phosphorylation of Kar9p by Cdc28p (Liakopoulos *et al.*, 2003; Maekawa *et al.*, 2003). From the daughter-bound SPB, Kip2p is thought to transport Kar9p toward the cMT plus end where it establishes contacts with the cortex through Myo2p (Beach *et al.*, 2000; Yin *et al.*, 2000; Hwang *et al.*, 2003; Maekawa *et al.*, 2003). By linking micro-

This article was published online ahead of print in *MBC in Press* (<http://www.molbiolcell.org/cgi/doi/10.1091/mbc.E05-06-0565>) on October 19, 2005.

□ The online version of this article contains supplemental material at *MBC Online* (<http://www.molbiolcell.org>).

Address correspondence to: Rita K. Miller (rmlr@mail.rochester.edu).

Abbreviations used: AD, activation domain; CFP, cyan fluorescent protein; cMT, cytoplasmic microtubule; DBD, DNA binding domain; HU, hydroxyurea; MAP, microtubule-associated protein; MT, microtubule; SPB, spindle pole body; TAP, tandem affinity purification.

tubules (MTs) from the older SPB to the bud cortex, Kar9p directs only that pole to the daughter cell.

Two B-type cyclins have been implicated in spindle positioning and the Cdc28p-dependent phosphorylation of Kar9p. Clb4p regulates the stability of astral MT interactions with the bud tip (Maekawa and Schiebel, 2004). Kar9p is required for Clb4p localization at the SPBs and MTs (Maekawa and Schiebel, 2004). Deletion of *CLB4* reduces the level of Kar9p phosphorylation and disturbs the restriction of Kar9p to the daughter-bound SPB (Liakopoulos *et al.*, 2003; Maekawa and Schiebel, 2004). A second B-type cyclin, *CLB5*, interacts with *KAR9* by two-hybrid analysis (Maekawa *et al.*, 2003) and in vitro phosphorylation assays suggest that Kar9p is a specific substrate of the Clb5p-Cdc28p kinase (Loog and Morgan, 2005). A *clb5Δ cdc28-4* double mutation also alters Kar9p localization on SPBs and at the cMT plus end (Maekawa *et al.*, 2003; Maekawa and Schiebel, 2004). Mutations in *clb5* affect spindle pole polarity and can result in both spindle poles being transported into the bud (Segal *et al.*, 1998, 2000b).

Previously, Kar9p has been shown to interact with three MT-associated proteins: Bim1p, Kip2p, and Stu2p (Korinek *et al.*, 2000; Lee *et al.*, 2000; Miller *et al.*, 2000; Maekawa *et al.*, 2003). In this study, we identify Bik1p as a fourth MT-associated protein (MAP) that interacts with Kar9p. Bik1p promotes MT stability and is a member of the CLIP-170 family of MT plus end-tracking proteins (Berlin *et al.*, 1990; Schuyler and Pellman, 2001). Mutations in either *BIK1* or *KIP2* result a similar phenotype of short cMTs, presumably because Kip2p can recruit Bik1p to cMT plus ends (Cottingham and Hoyt, 1997; Miller *et al.*, 1998; Carvalho *et al.*, 2004). The molecular explanation for the placement of Bik1p in the dynein genetic pathway is based on the finding that Bik1p functions in concert with Kip2p and the LIS1 homologue Pac1p to recruit dynein to the MT plus end (Lee *et al.*, 2003; Sheeman *et al.*, 2003; Carvalho *et al.*, 2004).

Here, we show a new role for Bik1p. Our data suggest that Bik1p is important for accurate SPB inheritance by directing the localization of Kar9p onto cMTs emanating from the older SPB, thus enabling them to interact with the bud cortex. Mechanistically, we propose that Bik1p influences Kar9p localization through a phosphorylation mechanism by regulating the interaction between Kar9p and the cyclin Clb5p. This represents a novel mechanism of regulation in which a MT binding protein affects the localization of a binding partner by modulating its phosphorylation.

MATERIALS AND METHODS

Yeast Strains and Growth Conditions

S. cerevisiae strains and plasmids used in this study are listed in Table 1. Primers and oligonucleotides used for strain constructions can be found in the online supplement (Table 1-S). Cells were grown in yeast peptone dextrose (YPD) or synthetic complete (SC) media as described previously (Miller *et al.*, 1999).

Two-Hybrid Assay

The two-hybrid system of James *et al.* (1996) was used. The *GAL4* DNA binding domain (DBD) plasmid pGBDU-C3 (James *et al.*, 1996) was modified by replacing the *Bgl*III site with a *Sac*I site. pGBDU-C3 was cut with *Bgl*III and oligonucleotides #38 and #39 containing the *Sac*I site were ligated in, creating pRM2345. This destroyed the original *Bgl*III site. Truncations of *KAR9* were amplified by PCR with terminal *Sall* and *Sac*I sites using the oligonucleotides listed in Table S1 and pRM381 as a template. These were cloned into the *Sall* and *Sac*I sites of pRM2345 and verified by sequencing. The truncation of *KAR9* containing amino acids 1–316 was generated by digestion of the full-length construct (pRM1493) with *Swa*I and *Pst*I to yield pRM2432. Full-length *KAR9* fused to the DBD (pRM1493/pMR4150) was generated as described previously (Miller *et al.*, 2000).

To generate a *BIK1* fusion with the *GAL4*-activation domain (AD), *BIK1* was synthesized by PCR with terminal *Eco*RI and *Bam*HI restriction sites using primers #59 and #60 and pDP65/B3102/pRM 493 as template. This product was cloned into the *Eco*RI and *Bam*HI sites of pGAD-C3/pRM1153 and verified by sequencing, generating pRM2627.

CLB5 was fused to the *GAL4* AD by ligating a 2.1-kb fragment excised with *Bam*HI and *Pst*I from pRM2340/BDU-C5.1 (a generous gift from Fred Cross, Rockefeller University, New York, NY) to pRM1151/pGAD-C1 cut with *Bam*HI and *Pst*I. This generated pRM2721, which lacks the first four amino acids of Clb5p.

CLB4 was amplified from the chromosomal locus by PCR with terminal *Eco*RI and *Bam*HI restriction sites using primers #344 and #345 and then cloned into the *Eco*RI and *Bam*HI sites of pGAD-C3/pRM1153 to generate pRM 5041 (wild-type AD-*CLB4*). Mutant *CLB4* was synthesized by PCR and cloned into the *Sall* and *Sac*I sites of pRM2603 to generate pRM4949, which contains the *CLB4* amino acid substitutions Q36R and I244M. These fusions were verified by sequencing.

DBD and AD plasmids were transformed into the yeast reporter strain PJ69-4A (yRM1757) (James *et al.*, 1996) and selected for growth on plates lacking uracil and leucine. Interactions were assayed by transferring cells with a multiprong transfer device to SC plates lacking uracil and leucine (–ura-leu) or histidine (–his). Growth was scored after incubation at 30°C for 2–3 d.

To generate a two-hybrid reporter strain disrupted for *BIK1*, pVB17 (B2134/pRM494) (Berlin *et al.*, 1990) was digested with *Sna*BI and *Eco*RI and transformed into PJ69-4A (yRM1757) (James *et al.*, 1996). Prototrophs were selected on SC plates lacking tryptophan. The disruption in yRM2258 was confirmed biochemically by Western blotting with α -Bik1p and phenotypically by scoring defects in nuclear positioning as described previously (Miller and Rose, 1998).

Affinity Chromatography

The glutathione S-transferase (GST) vector pGEX-4T-2 (GE Healthcare, Little Chalfont, Buckinghamshire, United Kingdom) was modified by replacing the *Not*I site in the multiple cloning site with *Sac*I, using oligonucleotides #72 and #73 to generate pRM2759. A fragment encoding the carboxy-terminal basic domain of Kar9p (amino acids 391–644) was synthesized by PCR with terminal *Sall* and *Sac*I ends and cloned into the *Sall* and *Sac*I of pRM2759 to produce pRM4167. This was verified by sequencing.

Expression of GST-Kar9^{391–644aa} and GST alone were induced in BL21(DE3) *Escherichia coli* (Stratagene, La Jolla, CA) using 1 mM isopropyl β -D-thiogalactoside (IPTG) at 37°C for 1.5 h. Cells were resuspended in PEM buffer (80 mM Pipes, pH 6.8, 1 mM MgCl₂, 1 mM EGTA, and protease inhibitors) and lysed by sonication. The crude bacterial lysates were centrifuged at 16,000 \times g at 4°C for 25 min. The supernatant was transferred to a fresh tube and centrifuged at 16,000 \times g at 4°C for 20 min. Bacterial lysate (1 mg) was added to a Microspin GST purification column (GE Healthcare) containing a 50- μ l bed of glutathione agarose and mixed for 30 min at 4°C. Unbound protein was removed from the beads by centrifugation at 837 \times g for 1 min. The beads were washed 20 times with 350 μ l of cold PEM buffer.

His₆-Bik1p expressed in BL21(DE3) bacteria was purified by nickel column chromatography, eluted with a step gradient of imidazole. The 350 mM imidazole fraction was dialyzed into PEM buffer, pH 6.8. Purified Bik1p (10 μ g) was added to spin columns containing bound with either GST-Kar9^{391–644aa} or GST alone and mixed for 30 min at 4°C. Unbound protein was cleared from the column by centrifugation at 837 \times g, followed by 25 washes with 600 μ l of cold PEM buffer. Bound proteins were eluted by the addition of 100 μ l of 10 μ M reduced glutathione and centrifugation.

TAP-tagging KAR9

Chromosomal *KAR9* was tagged at its carboxy terminus with a tripartite tandem affinity purification (TAP) tag consisting of 6x-histidine, hemagglutinin (HA), and protein A as described Puig *et al.* (2001). Briefly, the TAP tag and *Kluyveromyces lactis* *URA3* marker were amplified by PCR using primers #144 and #147 and the template pRM3175/AVA0258 (a generous gift from Eric Phizicky, University of Rochester, Rochester, NY). The amplified region included 50 terminal base pairs of homology to the 3' end of the *KAR9* locus and the downstream region, allowing for integration by homologous recombination. Recombinants were selected at 30°C on SC plates lacking uracil. The *KAR9-tap* fusion was verified by Western blot and PCR of genomic DNA. All *KAR9-tap* strains described in this study are derived from yRM3221.

To determine whether the *KAR9-tap* fusion was functional, we assayed for both nuclear positioning defects and synthetic lethality in crosses with mutants of the dynein pathway (Miller *et al.*, 1998). *KAR9-tap* (yRM3221) was crossed to *dym1Δ* (yRM672), *kip2Δ* (yRM666), and *bik1Δ* (yRM526/MS4734). *KAR9-tap* (yRM3379) was also crossed to *pac1Δ* (yRM3138/ATCC4002525, a nonisogenic cross). In each case, tetrad dissection produced 100% viable double mutants: *KAR9-tap dym1Δ* (15 of 15 predicted double mutants), *KAR9-tap bik1Δ* (11 of 11), *KAR9-tap kip2Δ* (17 of 17), and *KAR9-tap pac1Δ* (8 of 8). No difference was detected in the growth of the double mutant colonies in comparison to the single mutants or wild type. To test for nuclear positioning defects, *KAR9-tap* (yRM3221), wild type (yRM 2147), and *kar9Δ* (yRM433) strains were grown to mid-log phase in YPD media at 30°C, fixed in 75%

Table 1. *S. cerevisiae* strains and plasmids used in this study

	Genotype/comments	Source
Yeast strain		
yRM425	<i>MATa dyn1Δ::URA3 ura3-52 leu2-3 leu2-112 trp1Δ1 his3Δ200</i>	This study
yRM433/MS4306	<i>MATa kar9-Δ2::HIS3 leu2-3 leu2-112 ura3-52 ade2-101 his3Δ200</i>	Miller and Rose 1998
yRM526/MS4734	<i>MATα bik1Δ::TRP1 leu2-3 leu2-112 ura3-52, trp1Δ1</i>	Miller and Rose 1998
yRM565	<i>MATa bik1Δ::TRP1 leu2-3 leu2-112 ura3-52 trp1Δ1 ade2-101 his3Δ200</i>	This study
yRM666	<i>MATa kip2Δ::TRP1 leu2-3 leu2-112 ura3-52 trp1Δ1</i>	This study
yRM672	<i>MATα dyn1Δ::LEU2 leu2-3 leu2-112 ura3-52, trp1Δ1</i>	This study
yRM1757/PJ69-4A	<i>MATa trp1-901 leu2-3 leu2-112 ura3-52 his3Δ200 gal4Δ gal80Δ LYS2::GAL1-HIS3 GAL2-ADE2 met3::GAL7-lacZ</i>	James <i>et al.</i> 1996
yRM2060/MS7310	<i>MATa bim1Δ::Kan^R leu2-3 leu2-112 ura3-52 ade2-101 his3Δ200</i>	Miller <i>et al.</i> 2000
yRM2147/MS1556	<i>MATa leu2-3 leu2-112 ura3-52 ade2-101 his3Δ200</i>	Rose
yRM2146/MS52	<i>MATα leu2-3 leu2-112 ura3-52, trp1Δ1</i>	Rose
yRM2258	<i>MATa bik1Δ::TRP1 trp1-901 leu2-3 leu2-112 ura3-52 his3Δ200 gal4Δ gal80Δ LYS2::GAL1-HIS3 GAL2-ADE2 met3::GAL7-lacZ</i>	This study
yRM3138/ATCC4002525	<i>MATa pac1Δ::Kan^R leu2Δ1 ura3Δ his3Δ1 met15Δ</i>	American Type Culture Collection/Research Genetics
yRM3221	<i>MATa KAR9-tap::URA3 leu2-3 leu2-112 ura3-52 ade2-101 his3Δ200</i>	This study
yRM3379	<i>MATα KAR9-tap::URA3 leu2-3 leu2-112 ura3-52 trp1Δ1 ade2-101 his3Δ200</i>	This study
yRM3383	<i>MATa KAR9-tap::URA3 dyn1Δ::LEU2 leu2-3 leu2-112 ura3-52 trp1Δ1</i>	This study
yRM3442	<i>MATa KAR9-tap::URA3 bik1Δ::TRP1 leu2-3 leu2-112 ura3-52 ade2-101 his3Δ200</i>	This study
yRM3657	<i>MATα BIK1-3GFP::TRP1 leu2-3 leu2-112 ura3-52 trp1Δ1 [pAFS125C CFP-TUB1::URA3]</i>	This study
yRM3659	<i>MATα BIK1-3GFP::TRP1 kar9Δ-2::HIS3 leu2-3 leu2-112 ura3-52 trp1Δ1 his3Δ200 [pAFS125C CFP-TUB1::URA3]</i>	This study
yRM3681	<i>MATα KAR9-3GFP::TRP1 leu2-3 leu2-112 ura3-52 trp1Δ1</i>	This study
yRM3886	<i>MATα KAR9-3GFP::TRP1 leu2-3 leu2-112 ura3-52 trp1Δ1 [pAFS125C CFP-TUB1::URA3]</i>	This study
yRM4114	<i>MATa KAR9-tap::URA3 bim1Δ::Kan^R leu2-3 leu2-112 ura3-52 ade2-101 his3Δ200 trp1Δ1</i>	This study
yRM4122	<i>MATa KAR9-tap::URA3 kip2Δ::TRP1 leu2-3 leu2-112 ura3-52 trp1Δ1</i>	This study
yRM4261	<i>MATa KAR9-3GFP::TRP1 bik1Δ::TRP1 leu2-3 leu2-112 ura3-52 trp1Δ1 his3Δ200 [pAFS125C CFP-TUB1::URA3]</i>	This study
yRM4357	<i>MATα KAR9-3GFP::TRP1 SPC110-CFP::Kan^R leu2-3 leu2-112 ura3-52 trp1Δ1</i>	This study
yRM4358	<i>MATa KAR9-3GFP::TRP1 bik1Δ::TRP1 SPC110-CFP::Kan^R leu2-3 leu2-112 ura3-52 trp1Δ1 his3Δ200</i>	This study
yRM4366	<i>MATa KAR9-tap::URA3 bar1Δ::LEU2 leu2-3 leu2-112 ura3-52 trp1Δ1 his3Δ200</i>	This study
yRM4371	<i>MATα KAR9-3GFP::TRP1 kip2Δ::TRP1 leu2-3 leu2-112 ura3-52 trp1Δ1 [pAFS125C CFP-TUB1::URA3]</i>	This study
yRM4375	<i>MATα KAR9-3GFP::TRP1 kip2Δ::URA3 SPC110-CFP::Kan^R leu2-3, leu2-112 ura3-52 his3Δ200</i>	This study
yRM4568	<i>MATα BIK1-3GFP::TRP1 SPC110-DsRed::Kan^R leu2-3 leu2-112 ura3-52 trp1Δ1</i>	This study
yRM4598	<i>MATα KAR9-3GFP::TRP1 bik1Δ::TRP1 kip2Δ::URA3 SPC110-CFP::Kan^R leu2-3 leu2-112 ura3-52 trp1Δ1 his3Δ200</i>	This study
yRM4856	<i>MATa KAR9-tap::URA3 bik1Δ::KAN^R ura3⁻ leu2⁻ his3⁻ ade2-102 lys2Δ</i>	This study
yRM4863	<i>MATα KAR9-tap::URA3 bik1Δ::KAN^R ura3⁻ leu2⁻ his3⁻ ade2-102 lys2Δ trp1Δ</i>	This study
yRM4888	<i>MATα KAR9-tap::URA3 kip3Δ::HIS3 bar1Δ::LEU2 leu2-3 leu2-112 ura3-52 ade2-101 his3Δ200</i>	This study
yRM4951	<i>MATa SPC110-DsRed::Kan^R leu2-3 leu2-112 ura3-52 ade2-101 his3Δ200 [pAFS92 GFP-TUB1::URA3]</i>	This study
yRM4973	<i>MATa bik1Δ::TRP1 SPC110-DsRed::Kan^R leu2-3 leu2-112 ura3-52 trp1Δ1 ade2-101 his3Δ200 [pAFS92 GFP-TUB1::URA3]</i>	This study
yRM4978	<i>MATa kip2Δ::TRP1 SPC110-DsRed::Kan^R leu2-3 leu2-112 ura3-52 ade2-101 his3Δ200 [pAFS92 GFP-TUB1::URA3]</i>	This study
yRM5014	<i>MATα dyn1Δ::LEU2 SPC110-DsRed::Kan^R leu2-3 leu2-112 ura3-52 trp1Δ1 ade2-101 his3Δ200 [pAFS92 GFP-TUB1::URA3]</i>	This study
yRM5031	<i>MATα kar9Δ-2::HIS3 SPC110-DsRed::Kan^R leu2-3 leu2-112 ura3-52 trp1Δ1 ade2-101 his3Δ200 [pAFS92 GFP-TUB1::URA3]</i>	This study
yRM5119	<i>MATα KAR9-3GFP::TRP1 clb5Δ::URA3 SPC110-CFP::Kan^R leu2-3 leu2-112 ura3-52 trp1Δ1 ade2-101 his3Δ200</i>	This study
yRM5293	<i>MATα KAR9-3GFP::TRP1 kip3Δ::HIS3 leu2-3 leu2-112 ura3-52 trp1Δ1 his3Δ200 [pAFS125C CFP-TUB1::URA3]</i>	This study
yRM5301	<i>MATa KAR9-3GFP::TRP1 bik1Δ::TRP1 kip3Δ::HIS3 leu2-3 leu2-112 ura3-52 trp1Δ1 ade2-101 his3Δ200 [pAFS125C CFP-TUB1::URA3]</i>	This study

(Table continues)

Table 1. Continued

	Genotype/comments	Source
yRM5647	<i>MATa KAR9-3GFP::TRP1 bik1Δ::TRP1 clb5Δ::URA3 SPC110-CFP::Kan^R leu2-3 leu2-112 ura3-52 trp1Δ1 his3Δ200</i>	This study
yRM6007	<i>MATa kar9-S496A-3GFP::TRP1 SPC110-CFP::Kan^R leu2-3 leu2-112 ura3-52 trp1Δ1</i>	This study
yRM6015	<i>MATα kar9-S496A-tap::URA3 leu2-3 leu2-112 ura3-52, trp1Δ1</i>	This study
yRM6168	<i>MATα kar9-S197A-tap::URA3 leu2-3 leu2-112 ura3-52, trp1Δ1</i>	This study
yRM6170	<i>MATα kar9-S197A,S496A-tap::URA3 leu2-3 leu2-112 ura3-52, trp1Δ1</i>	This study
Plasmids		
pET-30+	Vector for tagging proteins with his ₆ KAN ^R	Novagen
pRM381/pMR3381	<i>KAR9 URA3 CEN yCP50 Amp^R</i>	Miller and Rose 1998
pRM493/pDP65/B3102	<i>BIK1 LEU2 CEN Amp^R</i>	Fink
pRM494/PVB17/B2134	<i>bik1::TRP Amp^R integration plasmid</i>	Fink
pRM514/pMR4722	<i>KAR9 HIS3⁺ 2μ Amp^R</i>	Miller <i>et al.</i> 2000
pRM516/pMR4723	<i>KAR9-HA HIS3⁺ 2μ Amp^R</i>	Miller <i>et al.</i> 2000
pRM1151	<i>GAD-C1 LEU2 2μ Amp^R</i>	James <i>et al.</i> 1996
pRM1153	<i>GAD-C3 LEU2 2μ Amp^R</i>	James <i>et al.</i> 1996
pRM1156	<i>GBDU-C3 URA3 2μ Amp^R</i>	James <i>et al.</i> 1996
pRM1493/pMR4150	<i>GBDU-KAR9 URA3 2μ</i>	Miller <i>et al.</i> 2000
pRM2149	<i>PGAL-BIK1-V5 URA3 2μ Amp^R</i>	Invitrogen
pRM2340/BDU-C5.1	<i>DBD-CLB5 URA3 2μ Amp^R</i>	Cross
pRM2345	<i>GBDU-C3 URA3 2μ with the BglII restriction site in the polylinker replaced with SacI</i>	This study
pRM2432	<i>GBDU-KAR9^{1-316aa} URA3 2μ Amp^R</i>	This study
pRM2480	<i>GBDU-KAR9^{1-279aa} URA3 2μ Amp^R</i>	This study
pRM2603	<i>GAD-C3 LEU2 2μ with the BglII restriction site in the polylinker replaced with SacI Amp^R</i>	This study
pRM2627	<i>GAD-BIK1 LEU2 2μ Amp^R</i>	This study
pRM2632	<i>GBDU-KAR9^{391-644aa} URA3 2μ Amp^R</i>	This study
pRM2633	<i>GBDU-KAR9^{200-644aa} URA3 2μ Amp^R</i>	This study
pRM2634	<i>GBDU-KAR9^{200-399aa} URA3 2μ Amp^R</i>	This study
pRM2719	<i>GBDU-KAR9^{391-470aa} URA3 2μ Amp^R</i>	This study
pRM2720	<i>GBDU-KAR9^{200-470aa} URA3 2μ Amp^R</i>	This study
pRM2721	<i>GAD-CLB5 LEU2 2μ Amp^R</i>	This study
pRM2730	<i>GBDU-KAR9^{117-644aa} URA3 2μ Amp^R</i>	This study
pRM2759	<i>pGEX-4T-2 with the NofI restriction site in polylinker replaced with SacI Amp^R</i>	This study
pRM2860	<i>his_{6x}-BIK1 KAN^R lacI</i>	This study
pRM2862	<i>GBDU-KAR9^{391-540aa} URA3 2μ Amp^R</i>	This study
pRM2863	<i>GBDU-KAR9^{471-644aa} URA3 2μ Amp^R</i>	This study
pRM2888	<i>GBDU-KAR9^{471-580aa} URA3 2μ Amp^R</i>	This study
pRM2889	<i>GBDU-KAR9^{471-613aa} URA3 2μ Amp^R</i>	This study
pRM2909	<i>GBDU-KAR9^{534-580aa} URA3 2μ Amp^R</i>	This study
pRM2951	<i>GBDU-KAR9^{117-297aa} URA3 2μ Amp^R</i>	This study
pRM3175/AVA0258	<i>A template for TAP-tagging with his_{6x}-HA-3C-ProteinA K.I. URA3</i>	Phizicky
pRM3634	<i>3GFP TRP1 Amp^R integration plasmid with Sall-XmaI-SacI sites in the polylinker</i>	This study
pRM3662	<i>KAR9^{117-644aa}-3GFP TRP1 Amp^R integration plasmid</i>	This study
pRM4167	<i>GST-KAR9^{391-644aa} Amp^R</i>	This study
pRM4335/pTY24	<i>pFA6a-DsRed.T1.N1-Kan-Mx6 Amp^R</i>	Yeast Resource Center
pRM4340/pDH3	<i>pFA6a-CFP-Kan-Mx6 Amp^R</i>	Yeast Resource Center
pRM4949	<i>GAD-clb4* (Q36R, I244M mutations) LEU2 2μ Amp^R</i>	This study
pRM5041	<i>GAD-CLB4 LEU2 2μ Amp^R</i>	This study
pRM5778	<i>kar9-S496A^{117-644aa}-3GFP TRP1 Amp^R integration plasmid</i>	This study
pRM6048	<i>kar9-S197A^{117-644aa}-3GFP TRP1 Amp^R integration plasmid</i>	This study
pRM6049	<i>kar9-S197A-S496A^{117-644aa}-3GFP TRP1 Amp^R integration plasmid</i>	This study
pRS426	<i>URA3 2μ Amp^R</i>	Sikorski
AFS125C	<i>pCFP-TUB1::URA3 Amp^R</i>	Straight
AFS92	<i>pGFP-TUB1::URA3 Amp^R</i>	Straight

methanol/25% acetic acid, and stained with 6-diamidino-2-phenylindole (DAPI). Nuclear positioning defects were scored as described previously (Miller *et al.*, 1998; Miller and Rose, 1998). The *KAR9-tap* strain exhibited the same percentage of binucleate mothers and unmigrated mitotic nuclei (1.8% of large-budded cells, n = 228) as wild type (1%, n = 202). This percentage was significantly lower than in *kar9Δ* (21%, n = 229). Combined, these results suggest that the function of the Kar9p-tap fusion protein has not been compromised.

Fluorescence Microscopy

To visualize Kar9p at endogenous protein levels, genomic *KAR9* was fused to three copies of green fluorescent protein (GFP) at its carboxy terminus. The

pBS-3xGFP-TRP1 vector (Lee *et al.*, 2003) was modified to include a *Sall*-*Xma*I-*Sac*I linker at the *Bam*HI site using the oligonucleotides #188 and #189, generating pRM3634. A fragment of *KAR9* (349–1932 bp) was synthesized by PCR to include a 3' triple Gly Ala linker and terminal *Sall* and *Sac*I sites using the primers #69 and #194. This was cloned into the *Sall*-*Sac*I sites of pRM3634 and verified by sequencing to create pRM3662. To integrate the 3xGFP tag at the *KAR9* locus, pRM3662 was linearized at the *Clal* site of *KAR9* and transformed into the wild-type strain, MS52/yRM2146 to generate yRM3681. Recombinants were selected on SC plates lacking tryptophan at 30°C. The functionality of *KAR9-3GFP* fusion was assayed by scoring for nuclear migration defects and synthetic lethality with mutants in the dynein pathway. *KAR9-3GFP* did not exhibit any obvious spindle positioning defects, as the

frequency of incorrectly migrated mitotic nuclei was similar to nontagged wild-type control (1.4%; $n = 215$). Additionally, *KAR9-3GFP* (yRM3681) was viable in double mutant combinations with *dyn1Δ* (yRM425, 18 of 18 predicted double mutants), *bik1Δ* (yRM565, 18 of 18), and *pac1Δ* (yRM3138/ATCC4002525, 14 of 14 in a nonisogenic cross). We conclude that *KAR9* tagged with 3xGFP tag is functional. All Kar9p-3GFP described in this study were derived from yRM3681.

To visualize MTs, CFP-Tub1 (pAFS125C; a gift from J. Cooper, Washington University Medical School, St. Louis, MO) was cut with *StuI* and integrated at the *URA3* locus, generating yRM 3886 and other strains. To identify the ends of cMTs, images above and below the Z-plane of the apparent MT end were examined.

SPC110 was tagged using the primers (#251 and #252) and templates as described previously (Yoder *et al.*, 2003). The cyan fluorescent protein (CFP) tag was constructed using the pDH3/pRM4340 template, and the red fluorescent protein (DsRed) tag was based on the pTY24/pRM4335 template (both gifts of the Yeast Resource Center, University of Washington, Seattle, WA).

Microscopy was carried out on a motorized Zeiss Axioplan 2 microscope equipped with a 100× Plan-Neofluor lens (1.3 numerical aperture) (Carl Zeiss, Thornwood, NY), a cooled charge-coupled device camera (ORCA-ER; Hamamatsu, Hamamatsu City, Japan), and Chroma and/or Zeiss filter sets. Images were acquired and processed using Openlab 3.5.2 software (Improvision, Lexington, MA).

Preparation of Bik1p Antibodies

A his₆-*BIK1* plasmid was generated by synthesizing *BIK1* by PCR with terminal *Bam*HI and *Hind*III sites using primers #80 and #79 and pDP65/pRM493 as template. This fragment was cloned into the *Bam*HI and *Hind*III sites of pET-30+ (Novagen, Madison, WI) to generate pRM2860. Expression of the his₆-Bik1p protein was induced in BL21(DE3) bacteria (Novagen) using 1 mM IPTG at 37°C for 3 h. Cells were lysed by sonication on ice in binding buffer (20 mM Tris, pH 8.0, 0.5 M NaCl, 5 mM imidazole, and 0.1% Triton). The fusion protein was isolated by nickel-affinity chromatography using a step gradient of imidazole. his₆-Bik1p eluted at 250 and 300 mM imidazole. Fractions were pooled, concentrated to 3.2 mg/ml in phosphate-buffered saline, and injected into New Zealand White rabbits (rabbit #2832; Harlan Bioproducts for Science, Indianapolis, IN). Serum (1:1000 dilution in 5% milk/phosphate-buffered saline) was preabsorbed on three Western blots of *bik1Δ* extract for 8 h each. Western blots of wild-type whole cell extracts probed with this serum yielded a single band at 51.1 kDa corresponding to the molecular weight of Bik1p that was not present in extracts from *bik1Δ* strains. Alternatively, IgG was purified on Bio-Rad DEAE cartridges (Bio-Rad, Hercules, CA) according to manufacturer's instructions.

Immunoprecipitations and Western Blotting

Protein extracts were prepared from cultures grown to mid-exponential phase. Cells were washed once with water, resuspended in cold B150 buffer (50 mM Tris, pH 7.4, 150 mM NaCl, and 0.2% Triton X-100) with protease inhibitors (Sigma protease inhibitor cocktail, 1 mM phenylmethylsulfonyl fluoride, CLAAP, E64, and bestatin), and lysed by vortexing with glass beads. Crude extracts were then clarified by centrifugation at 16,000 × *g* for 20 min. The supernatant was transferred to a fresh tube and centrifuged at 16,000 × *g* for 20 min.

Kar9p-HA was coimmunoprecipitated with Bik1p-V5 (Invitrogen, Carlsbad, CA) from exponentially growing cultures as previously described for Bim1p-V5 (Miller *et al.*, 2000), except that α-HA-conjugated agarose beads were from Santa Cruz Biotechnology (Santa Cruz, CA). Bik1p-V5 expression was induced by the addition of 2% galactose for 3 h.

To immunoprecipitate Bik1p, 3 μl of cartridge purified α-Bik1p was added to 1 ml of 3 mg/ml protein extract and incubated on a rotisserie at 4°C for 4 h. Protein A-Sepharose (5 μg; GE Healthcare) in 20 μl of B150 buffer was added and incubated on a rotisserie at 4°C for 1 h. The precipitate was then washed five times with cold B150 buffer. Bound proteins were eluted by the addition of 30 μl of 3× Laemmli buffer and boiled for 3 min. Then, 15 μl of each sample was analyzed after 8% SDS-PAGE by Western blotting.

For Western blotting, Kar9p-tap was detected with α-HA (Santa Cruz Biotechnology) at 1:200. Bik1p-V5 fusions were detected using α-V5 (Invitrogen) at 1:5000, and GST fusions were detected using α-GST (Sigma-Aldrich, St. Louis, MO) at 1:8000. Cartridge purified α-Bik1p was used at 1:750. Chicken α-actin was used at 1:20,000.

kar9 Mutants

Point mutations were introduced into the *KAR9-3GFP* plasmid (pRM3662) by site-directed mutagenesis using the QuikChange mutagenesis kit (Stratagene) to generate *kar9-S197A* (pRM6048), *kar9-S496A* (pRM5778), and *kar9-S197A S496A* (pRM6049) using the oligonucleotide pairs #427/#428 for S496A and #446/#447 for S197A. The absence of errors was confirmed by sequencing. These were integrated at the endogenous *KAR9* locus of the wild-type strain MS52/yRM2146 after digestion with the restriction enzyme *Cla*I. Each integration was confirmed by PCR and Western blotting. TAP-tagged versions of these mutants were created by integrating the TAP tag cassette for *KAR9* into

the corresponding GFP-tagged strains, replacing the 3GFP tag and *TRP+* marker. This generated *kar9-S197A-tap* (yRM6168), *kar9-S496A-tap* (yRM6015), and *kar9-S197A S496A-tap* (yRM6170).

Drug and Phosphatase Treatments

Nocodazole Treatment. Cultures were grown to early exponential phase in YPD media. Nocodazole (Sigma-Aldrich; 1.5 mg/ml stock solution in dimethyl sulfoxide [DMSO]) was added to a final concentration of 15 μg/μl at 30°C for 1.5 h. An equivalent volume of DMSO was added to a separate culture as a mock experiment. Depolymerization of MTs was confirmed by indirect immunofluorescence as described previously (Miller, 2004). Less than 0.5% of treated cells displayed any α-tubulin staining.

Hydroxyurea Treatment. Cultures were grown to early exponential phase in YPD media. Hydroxyurea (HU) (Sigma-Aldrich) was added to a final concentration of 100 mM at 30°C for 2 h. Bud morphology was used to demonstrate that >98% of cells were arrested in late S phase.

Phosphatase Treatment. Protein extracts were prepared from asynchronous mid-log cultures. λ Phosphatase (800 U; New England Biolabs, Beverly, MA) was added to 150 μg of extract (in B150 buffer containing 2 mM MnCl₂ with 1× phosphatase buffer) and incubated at 30°C for 30 min. As a negative control, extracts were incubated without enzyme under identical reaction conditions.

RESULTS

Kar9p Physically Interacts with Bik1p

Because Kar9p interacts with several MAPs, we tested whether Kar9p might also interact with the CLIP-170 homologue Bik1p. To assay for this interaction, Kar9p was immunoprecipitated from a strain in which Kar9p was tagged with the HA epitope and Bik1p-V5 was expressed under the control of the *GAL1* promoter as described previously (Miller *et al.*, 2000). As shown in Figure 1A, Bik1p-V5 was present in the precipitate, indicating that the two proteins interact physically. Because Bik1p also interacts with Bim1p (Ito *et al.*, 2001) (our unpublished observations), we asked whether Bik1p-V5 could be associating indirectly with Kar9p through a tertiary complex with Bim1p. To test this possibility, we repeated the Kar9p immunoprecipitation in *bim1Δ* cells. Bik1p-V5 again coimmunoprecipitated specifically with Kar9p-HA (Figure 1A). Thus, the Kar9p-Bik1p interaction is not dependent on Bim1p.

To identify the domain of Kar9p to which Bik1p binds, we used a two-hybrid approach. Full-length *KAR9* (1–644 aa) and three truncations corresponding to the acidic (1–316 aa), coiled-coil (200–399 aa), and basic domains (391–644 aa) were tested for interaction with *BIK1*. As shown in Figure 1B, *BIK1* interacted with both full-length and the basic domain of Kar9p but not with the acidic or coiled-coil fragments, suggesting that Kar9p binds to Bik1p through its basic domain. The interactions were readily detected using *HIS3* as the reporter but were weak using the more stringent reporter *ADE2*, explaining why previous screens did not detect this interaction (Miller *et al.*, 2000; Ito *et al.*, 2001).

We next wanted to determine whether the interaction between Bik1p and Kar9p was direct. The basic domain of Kar9p (391–644 aa) was fused to GST, expressed in *E. coli*, and purified on glutathione agarose. his₆-Bik1p was expressed in *E. coli*, purified by nickel column chromatography, and applied to columns of either the GST-Kar9p^{391–644aa} fusion (lane 2) or GST alone (lane 3). As shown in Figure 1C, elution with reduced glutathione revealed that his₆-Bik1p bound to GST-Kar9p^{391–644aa} but not GST alone. Thus, the interaction between Kar9p and Bik1p occurs through the basic domain of Kar9p and does not require an intervening protein.

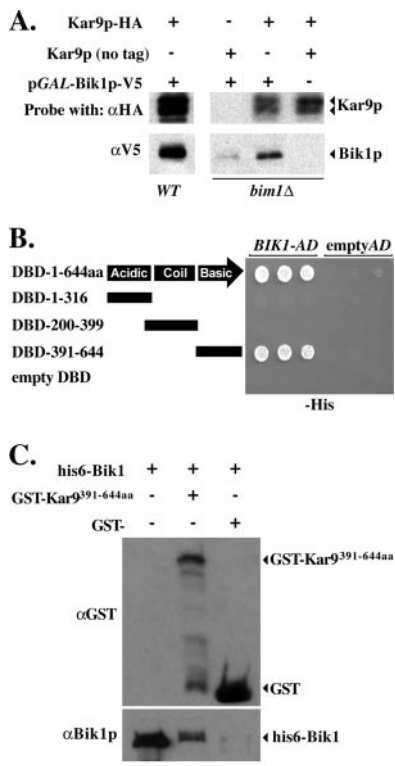


Figure 1. Bik1p binds directly with the basic domain of Kar9p. (A) Coimmunoprecipitation. Kar9p-HA was immunoprecipitated with α -HA-conjugated agarose beads from extracts of wild-type (yRM2147) and *bim1* Δ (yRM2060) strains. Each strain contained the indicated plasmids: Kar9p-HA on a 2 μ plasmid (pRM516), non-tagged KAR9 (pRM514), pGAL-BIK1-V5 (pRM2149), or empty vector (pRS426). The presence of Bik1p in the precipitate was detected using α -V5. The two forms of Kar9p seen here are not comparable with the three forms seen in later experiments because a different percentage of gel and a different epitope tag were used for this experiment. (B) Two-hybrid analysis. Full-length KAR9 (pRM1493) and three truncations of KAR9 fused to the GAL4-DNA binding domain. 1–316 aa (pRM 2432), 200–399 aa (pRM2634), and 391–644 aa (pRM2632) were assayed for interaction with BIK1 fused to the GAL4-activation domain (pRM2627) in the two-hybrid reporter strain PJ69-4A. Three independent colonies were spotted onto plates lacking histidine (–his) and scored for growth at 30°C after 3 d (see *Materials and Methods*). Growth was equivalent for all spots on plates lacking uracil and leucine to demonstrate the presence of both plasmids (our unpublished data). (C) Direct binding. Either GST alone (pRM2759) or the basic domain of Kar9p (391–644aa) fused to glutathione S-transferase (pRM4167) was harvested from bacteria and bound in glutathione agarose columns (see *Materials and Methods*). Bacterially expressed his₆-Bik1p was purified by nickel column chromatography, and 10 μ g was added to columns of either GST-Kar^{391-644aa} (lane 2) or GST alone (lane 3). Bound proteins were eluted by the addition of reduced glutathione (lanes 2 and 3) and prepared for Western blotting. Lane 1 represents 1/5 of the his₆-Bik1p that was loaded onto the GST-Kar9p beads.

Bik1p and Kip2p Are Not Required for Kar9p Localization at the Plus End

Bik1p plays a role in recruiting dynein to the plus ends of cMTs (Sheeman *et al.*, 2003; Carvalho *et al.*, 2004). To test whether Bik1p might act similarly to focus Kar9p at plus ends, endogenous levels of a functional Kar9p-3GFP (see *Materials and Methods*) were visualized in both wild-type and *bik1* Δ cells containing cMTs visualized with CFP-labeled α -tubulin. We assayed whether Kar9p was present at three

sites within the cell, at the SPB, along the microtubule, and at the plus end of the cMT. Because Kar9p can exist at multiple locations simultaneously, cells were scored for combinations of these localizations (Table S2). When the localization of Kar9p at the plus end of the MT was analyzed (Figure 2B), irrespective of its localization at other sites, 74% of wild-type preanaphase cells were found to display a dot of Kar9p localization at the plus end ($n = 251$). When localization at the SPB was analyzed, irrespective of whether it was present at the plus end, 64% of wild-type cells displayed Kar9p at the SPB (Figure 2B). Forty-three percent of wild type displayed Kar9p at both sites (Table S2). Because *bik1* Δ strains contain shorter MTs, we scored the subset that contained cMTs long enough to clearly permit the distinction between the SPB and the plus end. For this assay, however, the average length of cMTs remained shorter in *bik1* Δ than in wild type. The selected cMTs in preanaphase *bik1* Δ cells had a mean length of 1.24 ± 0.034 (SEM) μ m ($n = 103$), whereas the mean length of all cMTs in preanaphase *bik1* Δ cells was 0.84 ± 0.03 (SEM) μ m ($n = 173$). The average length of microtubules in wild type was 1.57 ± 0.055 (SEM) μ m ($n = 110$), a statistically significant difference. Kar9p-3GFP was present at the plus ends of cMTs in 85% of *bik1* Δ cells ($n = 250$), (Figure 2, A and B). Thus, Bik1p is not required for the localization of Kar9p at the plus end.

Whereas Kar9p was only seen along the MT in 13% of wild type, in 44% of *bik1* Δ cells Kar9p was distributed along the MT. To further confirm this mislocalization in *bik1* Δ cells, we sought to increase MT length in the *bik1* Δ background by using a *kip3* Δ mutation (DeZwaan *et al.*, 1997; Miller *et al.*, 1998). In a *kip3* Δ *bik1* Δ double mutant, the average length of cMTs analyzed was 1.77 ± 0.064 (SEM) μ m ($n = 109$). In 48% of these cells, Kar9p-3GFP was also distributed along cMTs (Figure 2B). In the *kip3* Δ single mutant, Kar9p localization was found along the MT in 32% of cells. Because microtubules can be extremely long in *kip3* Δ , cells were selected for this analysis in which the MTs did not curl along the inside of the bud cortex. The average length of the MTs analyzed in *kip3* Δ was 2.08 ± 0.061 (SEM) μ m ($n = 146$). Thus, the localization of Kar9p is more dispersed along the MT in *bik1* Δ mutants. In a converse experiment, we sought to determine whether Kar9p affected the plus end localization of Bik1p. Bik1p-3GFP localization was examined in strains deleted for KAR9. In 99% of preanaphase *kar9* Δ cells ($n = 157$), Bik1p-3GFP was found as a dot at the plus end of cMTs, compared with 94% in wild-type cells ($n = 152$) (Figure S2A). Therefore, Kar9p is not required for the plus end binding of Bik1p.

Because mutations in KIP2 also result in short cMTs and Kip2p is thought to be responsible for the transport of Kar9p to the plus end of the cMT, we examined Kar9p localization in *kip2* Δ mutants. For this assay, the average length of cMTs scored was 1.19 ± 0.036 μ m (mean \pm SEM; $n = 107$). The average length of all MTs was 0.68 ± 0.03 (SEM) μ m ($n = 192$). Consistent with previous reports (Maekawa *et al.*, 2003), 87% of *kip2* Δ cells displayed a concentrated focus of Kar9p at the SPB. However, 60% of *kip2* Δ cells also showed some Kar9p-3GFP localized at the plus end of MTs (Figure 2, A and B). Forty-seven percent displayed Kar9p localizations at both sites (Table S2). Typically, the dot at the SPB was brighter than the dot at the plus end. Thus, Kip2p enhances the localization of Kar9p at the plus end, but it is not required for its localization there.

Kar9p Localizes to Both SPBs in *bik1* Δ Strains

Previous studies have shown that Kar9p associates asymmetrically with the daughter-bound spindle pole (Liakopou-

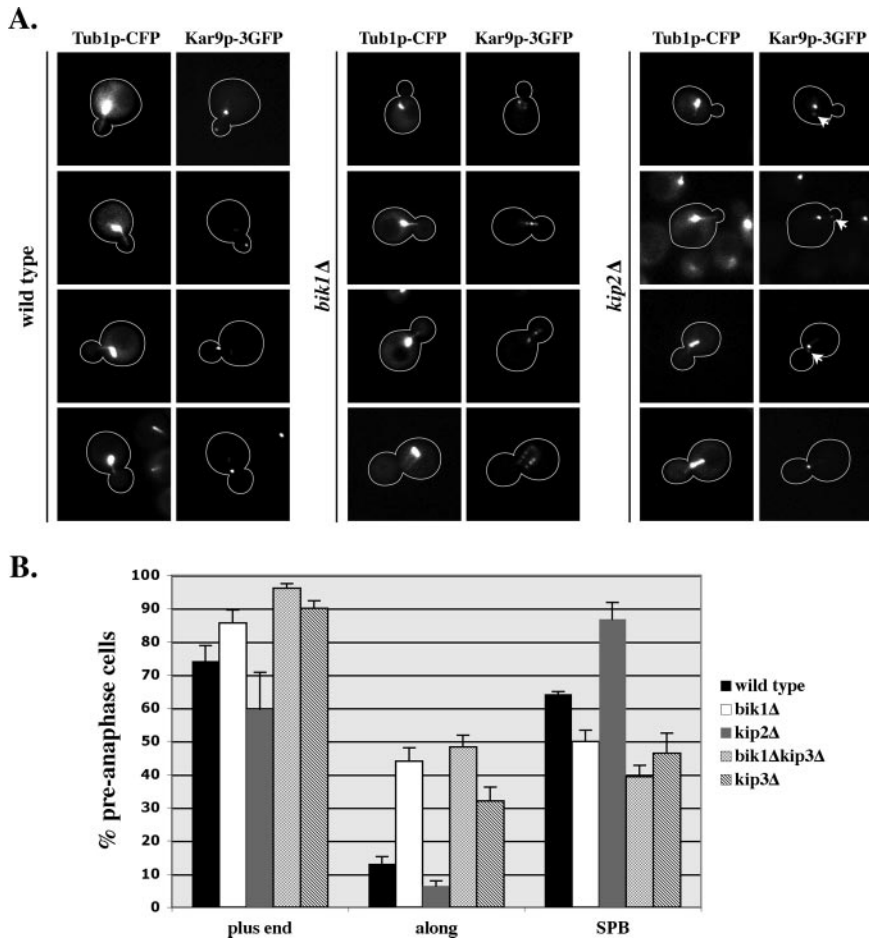


Figure 2. Localization of Kar9p-3GFP on cMTs in mutants. (A) Examples of Kar9p-3GFP localization in preanaphase wild-type, *bik1Δ*, and *kip2Δ* cells expressing Tub1p-CFP-labeled MTs. Arrowheads point to the Kar9p dot at the plus end of the cMT in *kip2Δ* cells. (B) Quantification of Kar9p-3GFP localization. “Plus end” represents the cells in which any Kar9p-3GFP was detected at the plus ends of cytoplasmic microtubules. “Along” represents cells in which Kar9p-3GFP could be seen along the length of the microtubule. “SPB” represents cells in which Kar9p-3GFP was observed at the minus end of cytoplasmic microtubules, near the spindle pole body. Cells in which Kar9p-3GFP was observed at multiple locations were scored in multiple categories. Kar9p-3GFP localization was scored in wild type (yRM3886; n = 252), *bik1Δ* (yRM4261; n = 250), *kip2Δ* (yRM4371; n = 250), *bik1Δ kip3Δ* (yRM5301; n = 251), and *kip3Δ* (yRM5293; n = 250) strains. Cells were grown in SC media –TRP at 30°C. Error bars denote the SEM of the percentages calculated in five separate experiments.

los *et al.*, 2003; Maekawa *et al.*, 2003). Because Bik1p also localizes to SPBs (Lin *et al.*, 2001; Carvalho *et al.*, 2004), we asked whether Bik1p might alter the localization of Kar9p at the SPB. Kar9p-3GFP localization was scored in wild-type and *bik1Δ* strains containing the SPB marker Spc110p-CFP. As expected, Kar9p-3GFP localized to one SPB in 69% of wild-type cells with short bipolar spindles (Figures 3 and S3) (Liakopoulos *et al.*, 2003; Maekawa *et al.*, 2003). In contrast, Kar9p-3GFP was localized to one pole in only 29% of *bik1Δ* cells. Instead, 70% of these cells display Kar9p on both SPBs (Figures 3 and S3). The majority of these cells displayed a slightly stronger GFP signal at one of the two poles. This suggests that Bik1p acts to restrict Kar9p localization to the daughter-bound SPB.

Bik1p localizes to a region associated with both SPBs in diploid cells (Lin *et al.*, 2001). Therefore, it seemed unlikely that in haploids Bik1p would promote Kar9p asymmetry by localizing to one SPB only. To further discount this possibility, we monitored the localization of Bik1p-3GFP in cells with SPBs labeled with Spc110p-DsRed. Bik1p-3GFP was always localized in a region associated with both SPBs in cells with short bipolar spindles (n = 150; Figure S2B). Thus, the localization of Bik1p itself does not explain the asymmetry of Kar9p, and additional factors are also probably involved.

Because mutations in Kip2p and Bik1p result in several similar phenotypes, we next tested whether Kip2p would have the same effect on Kar9p localization at the SPB. As shown in Figure 3B, Kar9p-3GFP was restricted to one SPB in *kip2Δ* cells at nearly the same frequency as seen in wild

type. This suggests that Kip2p and Bik1p provide separate functions for Kar9p.

If Bik1p functions to restrict Kar9p localization to the daughter-bound SPB before its transport to MT plus ends by Kip2p, then the localization of Kar9p-3GFP to both SPBs seen in *bik1Δ* should be epistatic to the asymmetric localization seen in *kip2Δ*. Indeed, the localization of Kar9p in *bik1Δ kip2Δ* strains was similar to that seen in *bik1Δ*, supporting the model that Bik1p functions before Kip2p with respect to Kar9p (Figure 3B).

Bik1p Functions in the Kar9p-dependent Mechanism of SPB Inheritance

In >90% of wild-type cells, the old SPB is inherited by the daughter cell and the new SPB is retained in the mother (Pereira *et al.*, 2001; Yoder *et al.*, 2003). Current models postulate that the asymmetric localization of Kar9p to one SPB is important for accurate SPB inheritance (Liakopoulos *et al.*, 2003). Our finding that Kar9p localized to both SPBs in *bik1Δ* cells suggested that either pole may be directed toward the bud, in which case *bik1Δ* cells should also display a defect in SPB inheritance.

To test this hypothesis, SPB inheritance was analyzed using methods similar to those described by Pereira *et al.* (2001), except that we labeled the SPB component *SPC110* with a slow-folding form of the DsRed chromophore (Yoder *et al.*, 2003). This allowed the relative age of either SPB to be distinguished in cells with bipolar spindles. The old SPB displays a brighter Spc110p-DsRed signal, resulting from the

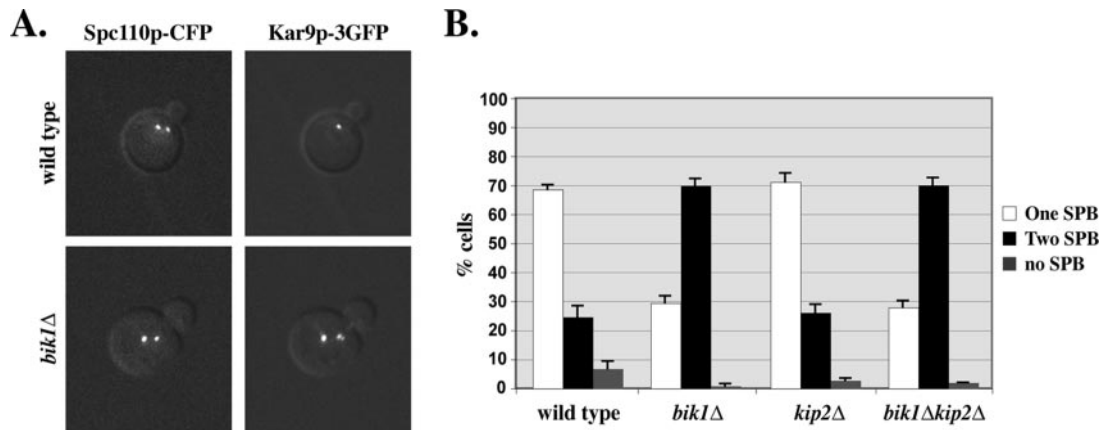


Figure 3. Bik1p restricts Kar9p to one SPB. (A) Kar9p-3GFP was localized in wild-type and *bik1Δ* strains containing SPBs labeled with Spc110p-CFP. Composites are shown of differential interference contrast with either GFP or CFP single images. (B) Quantification of Kar9p-3GFP at SPBs in wild-type (yRM4357; n = 277), *bik1Δ* (yRM4358; n = 289), *kip2Δ* (yRM4375; n = 252), and *bik1Δkip2Δ* (yRM4598; n = 153) cells with short bipolar spindles. Cells were grown in SC media –TRP at 30°C. Error bars denote the SEM of the percentages calculated in at least three separate experiments.

increased time allowed at this SPB for the DsRed-fluor to mature. The new SPB is therefore dimmer than the old SPB. To visualize the spindle, MTs were labeled with GFP (*GFP-TUB1*). Cultures were grown to stationary phase to allow for the accumulation of a bright DsRed signal at the undupli-

cated SPB and then released into fresh media for 2–3 h to allow SPB duplication and progression through the cell cycle. In 91% of wild-type cells with bipolar spindles aligned parallel to the mother-bud axis, the brighter SPB was oriented toward the bud (Figure 4). In cells lacking Kar9p, only 52% of the bud-

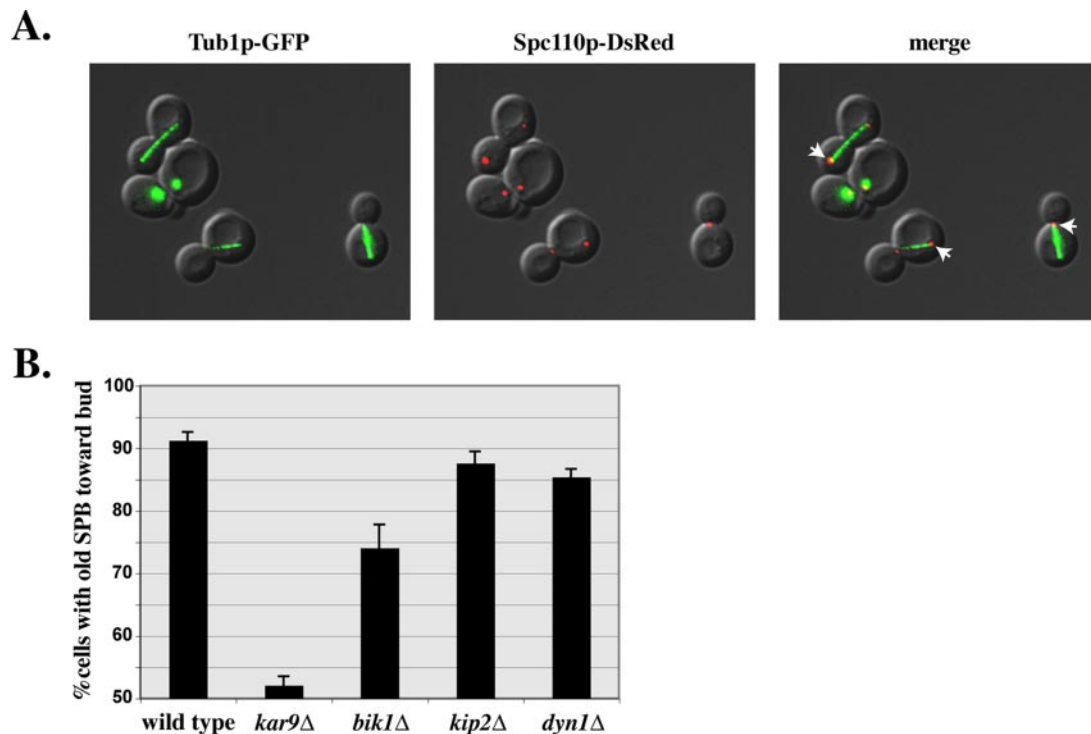


Figure 4. Bik1p has a function in SPB inheritance. (A) *bik1Δ* cells expressing Tub1p-GFP and SPBs labeled with Spc110p-DsRed. Composites are shown of differential interference contrast with either GFP or DsRed single images. Arrowheads point to the brighter and therefore older SPB. (B) Quantification of cells with the older SPB proximal to the bud in wild type (yRM4951; n = 480), *kar9Δ* (yRM5031; n = 359), *bik1Δ* (yRM4973; n = 409), *kip2Δ* (yRM4978; n = 324), and *dyn1Δ* (yRM5014; n = 158). Only cells with a bipolar spindle oriented along the long axis of the mother-bud were scored. The origin was set at 50% because this represents random inheritance. Error bars represent the SEM of the percentages obtained from at least three experiments. Fisher's exact test shows that the differences between the following pairs are statistically significant: *bik1Δ-kip2Δ* (two-tailed $p < 0.0001$), *dyn1Δ*-WT ($p = 0.0477$), *bik1Δ*-WT ($p < 0.0001$), and *bik1Δ-dyn1Δ* ($p = 0.0036$). The *kip2Δ-dyn1Δ* ($p = 0.565$) and *kip2Δ*-WT ($p = 0.1220$) pairs are not statistically different.

proximal SPBs displayed the brighter SPB signal. These findings are in close agreement with previous work suggesting that SPB inheritance is nearly random in *kar9Δ* strains (Pereira *et al.*, 2001). In *bik1Δ* cells, 74% of the brighter SPBs were directed toward the bud, representing a defect of 26%.

We also examined *kip2Δ* cells for defects in SPB inheritance. In 88% of *kip2Δ* cells, the brighter SPB signal was proximal to the bud. This suggests that the SPB inheritance defect in *bik1Δ* mutants is not solely the result of short cMTs. Moreover, 85% of *dyn1Δ* mutants displayed the correct SPB inheritance. Thus, *bik1Δ* mutants have a defect in SPB inheritance that is more severe than that observed in mutants of the dynein pathway but not as severe as *kar9Δ* mutants. These data are consistent with a model in which the effect of Bik1p on SPB inheritance is due largely to its effects on Kar9p localization.

Bik1p Binds both Phosphorylated and Unphosphorylated Kar9p

The Kar9p localization defects found in *bik1Δ* strains shown here were similar to those observed in *cdc28/cyclin* mutants and in *kar9* alleles with mutated phosphorylation sites (Liakopoulos *et al.*, 2003; Maekawa *et al.*, 2003). This suggested that the pattern of Kar9p mislocalization observed in *bik1Δ* could be related to its phosphorylation status. To test whether Bik1p might interact specifically with one isoform of Kar9p, we incorporated a TAP tag at the 3' end of the chromosomal *KAR9* locus (see *Materials and Methods*). Kar9p-tap was observed as a triplet in cellular extracts from asynchronously growing wild-type cultures (Figure 5). Bik1p was immunoprecipitated using a polyclonal Bik1p antibody and the precipitate was probed for Kar9p-tap using α -HA. As shown in Figure 5A, lane 2, all three Kar9p-tap isoforms coimmunoprecipitated with Bik1p. An identical immunoprecipitation in a *bik1Δ* strain containing Kar9p-tap showed little or no Kar9p-tap in the precipitate (lane 5). Therefore, the Bik1p antibody did not interact significantly with the TAP tag of Kar9p. This suggests that the Bik1p-Kar9p interaction is not dependent on the phosphorylation state of Kar9p.

Kar9p Is Hypophosphorylated in bik1Δ Mutants

We next examined the idea that Bik1p may function upstream of Cdc28p as part of the mechanism that leads to Kar9p phosphorylation. This predicts that Kar9p would be underphosphorylated in *bik1Δ* cells. To test this, we compared the isoforms of Kar9p-tap in wild-type and *bik1Δ* strains by Western blotting. The highest molecular weight isoform of the Kar9p-tap triplet was absent or greatly diminished in *bik1Δ* cells, with the two lower forms still present (Figure 5B). To eliminate the possibility that this might be a strain specific phenomenon, we confirmed that Kar9p was also hypophosphorylated in *bik1Δ* obtained from Research Genetics (our unpublished observations). Treatment with λ phosphatase reduced both the Kar9p-tap triplet in wild type and the doublet in *bik1Δ* to single bands (Figure 5C). Therefore, the two higher molecular weight bands are phosphorylated isoforms of Kar9p.

We next asked whether normal-length MTs were required for Kar9p phosphorylation. We first assayed for the presence of Kar9p isoforms in *kip2Δ* strains. As shown in Figure 5B, all three phospho-isoforms of Kar9p were present in *kip2Δ*, suggesting that short MTs do not affect Kar9p phosphorylation. To eliminate MTs using a different approach, cells were treated with nocodazole. This resulted in Kar9p hyperphosphorylation (Figure 5D). Although the interpretation of this result is confounded by the concomitant M-phase arrest

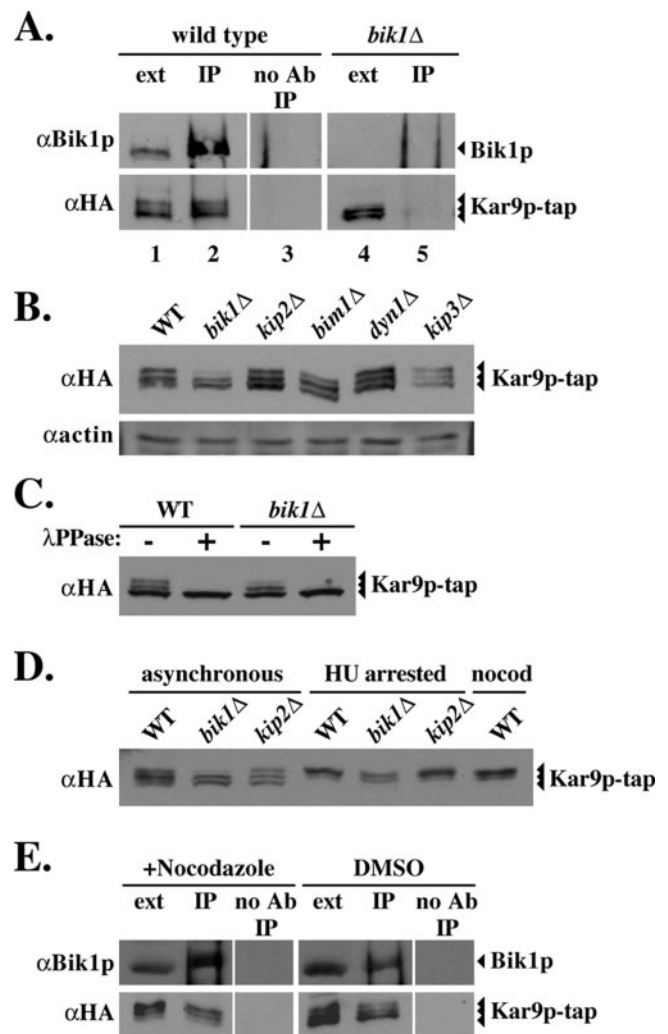


Figure 5. Bik1p promotes Kar9p phosphorylation. (A) Bik1p was immunoprecipitated using rabbit α -Bik1p and protein A-Sepharose from exponentially growing wild-type (yRM4366) or *bik1Δ* (yRM3442) strains expressing *KAR9-tap*. The tripartite TAP tag consists of his₆, HA, and protein A epitopes. The no-antibody control represents a mock immunoprecipitation carried out concurrently using protein A-Sepharose beads alone. The precipitates were analyzed by immunoblotting with α -HA to detect Kar9p-tap and rabbit α -Bik1p. Extracts from *KAR9-tap* and *bik1Δ* strains were run for comparison. The vertical lines in the control lanes are likely to be the result of the protein A used in the precipitations. (B) Extracts were prepared from wild-type (yRM4366), *bik1Δ* (yRM3442), *kip2Δ* (yRM4122), *bim1Δ* (yRM4114), *dyn1Δ* (yRM3383), and *kip3Δ* (yRM4888) strains each containing *KAR9-tap*. Cultures were grown to mid-exponential phase, lysed, and extracts were prepared for immunoblotting with α -HA. Actin was used as a loading control. (C) Protein extracts from wild-type and *bik1Δ* cells were treated with λ phosphatase or mock treated with no enzyme (see *Materials and Methods*) and prepared for immunoblotting. (D) Wild-type, *bik1Δ*, and *kip2Δ* strains expressing *KAR9-tap* were grown to early exponential phase, treated with HU, and extracts were prepared for immunoblotting. Wild type was also treated with nocodazole. (E) The interaction between Kar9p and Bik1p does not require MTs. Bik1p was immunoprecipitated with α -Bik1p from wild-type strains expressing *KAR9-tap* treated with nocodazole or with the DMSO solvent for 1.5 h. The two highest phosphorylated species of Kar9p-tap were apparent in extracts made from cells treated with nocodazole because Kar9p phosphorylation is increased at G₂/M (Maekawa *et al.*, 2003). λ PPase, λ phosphatase; nocod, nocodazole; WT, wild type; ext, extract; IP, immunoprecipitate.

caused by the nocodazole, it nevertheless indicates that the presence of MTs is not required for Kar9p phosphorylation. To determine whether long cMTs might alter Kar9p phosphorylation, we examined strains deleted for *KIP3* (DeZwaan *et al.*, 1997; Miller *et al.*, 1998). The isoforms in wild type and *kip3Δ* mutants were similar, each containing three isoforms (Figure 5B). This suggests that MT length does not regulate Kar9p phosphorylation.

To further discount the possibility that other spindle positioning mutants might alter Kar9p phosphorylation, we examined strains deleted for dynein and Bim1p. The higher molecular weight species was present in both the *dyn1Δ* and *bim1Δ* mutants (Figure 5B). Together, these data suggest that the *bik1Δ* mutation uniquely affects the phosphorylation state of Kar9p.

Kar9p phosphorylation is increased during late S phase (Liakopoulos *et al.*, 2003; Maekawa *et al.*, 2003). To determine whether the highest molecular weight species would be enhanced in *bik1Δ* mutants during S phase, we arrested wild-type and *bik1Δ* strains with HU. As shown in Figure 5D, the majority of Kar9p-tap was present in the highest molecular weight isoform in extracts made from HU-treated wild-type cells. In the *bik1Δ* mutant, the highest molecular weight band was also enhanced by HU treatment but not to the extent seen in wild type or *kip2Δ*. This suggests that the phosphorylation event resulting in the highest molecular weight band is not absolutely dependent upon Bik1p but that Bik1p contributes to this event.

The Interaction between Kar9p and Bik1p Does Not Require cMTs

To determine whether the Kar9p–Bik1p interaction requires the MT association of Bik1p, Bik1p was immunoprecipitated from *KAR9-tap* strains treated with nocodazole. The loss of MTs was confirmed by indirect immunofluorescence. As shown in Figure 5E, Kar9p-tap was present in the α -Bik1p precipitate of nocodazole-treated cells but not in the no-antibody control.

BIK1 Is Required for the Interaction between CLB5 and Full-Length KAR9

One explanation for the decreased level of Kar9p phosphorylation in *bik1Δ* mutants is that Bik1p promotes Kar9p phosphorylation by facilitating an interaction between Kar9p and a cyclin. To test this, we asked whether the two-hybrid interaction between *KAR9* and cyclins *CLB5* or *CLB4* required *BIK1*. As shown in Figure 6A, the *CLB5-KAR9* interaction was detected in the wild-type two-hybrid reporter strain but not in the reporter strain deleted for *BIK1*. We did not detect a two-hybrid interaction between *KAR9* and wild-type *CLB4* (Figure 6B). However, *KAR9* interacted strongly with a mutant form of *CLB4* containing two amino acid substitutions (Q36R and I244M), consistent with the possibility that these mutations may stabilize a weak or transient interaction. This interaction was not affected by the deletion of *BIK1* from the reporter strain (Figure 6B). This suggests that Bik1p is required for the Kar9p–Clb5p interaction but not the Kar9p–Clb4p interaction. These data provide additional evidence that the role of the S-phase cyclin *CLB5* is distinct from that of the mitotic cyclin *CLB4* with respect to the regulation of spindle positioning.

The requirement for *BIK1* in the two-hybrid interaction between *KAR9* and *CLB5* raises the possibility that Bik1p may interact with Clb5p. However, we were unable to detect a two-hybrid interaction between *CLB5* and *BIK1*, regardless of the DBD or AD fusion combination used or whether haploids or diploids were used as the reporter strain (our

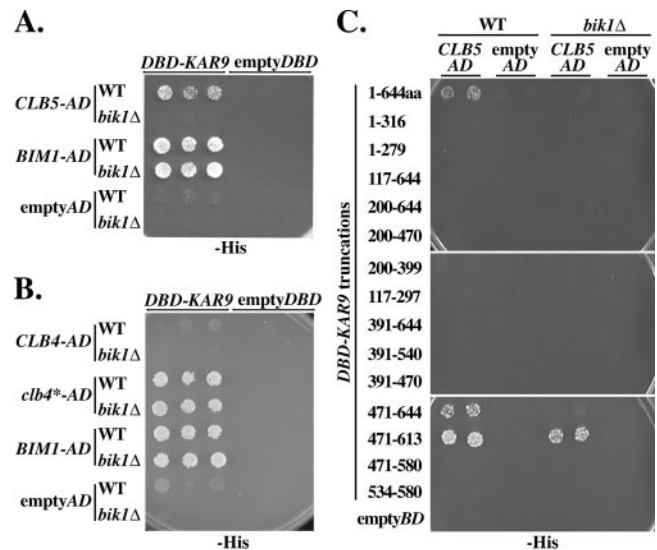


Figure 6. The interaction between *CLB5* and full-length *KAR9* requires *BIK1* by two-hybrid analysis. (A) Full-length *KAR9* fused to the *GAL4*-DBD (pRM1493) was assayed for interaction with *CLB5* fused to the *GAL4*-AD (pRM2721) in a wild-type two-hybrid reporter strain (PJ69-4A) and in a two-hybrid reporter strain in which *BIK1* was disrupted (yRM2258). Three independent colonies were spotted onto SC plates lacking histidine (–his). *BIM1*-AD was used as a positive control in both strains. Growth was equivalent for all spots on plates lacking uracil and leucine to demonstrate the presence of both plasmids (our unpublished data). (B) The wild-type *CLB4*-AD (pRM5041) and mutant *clb4^{ts}*-AD (pRM4949) plasmids were analyzed for interaction with *KAR9* fused to the DBD as described for A. *CLB4* in the *clb4^{ts}*-AD plasmid contains two amino acid substitutions, Q36R and I244M. (C) *CLB5* interacts with amino acids 471–613 encoded by *KAR9*. The *CLB5*-activation domain fusion was tested for interaction against a series of *KAR9* truncations fused to the *GAL4*-DBD in both the wild-type and *bik1Δ* reporter strains.

unpublished data). However, *GAL4* fusions with *BIK1* could conceivably confer steric interferences to Clb5p binding.

Another way in which Bik1p could facilitate the interaction between Kar9p and Clb5p would be for Bik1p to make Kar9p accessible to Clb5p, perhaps by relieving a steric hindrance present in full-length Kar9p. We reasoned that truncating Kar9p to the minimal region that supports an interaction with Clb5p might relieve this putative steric hindrance. Therefore, we used a two-hybrid mapping strategy to identify a region of *KAR9* corresponding to amino acids 471–613 that was sufficient for interaction with *CLB5* (Figure 6C). This interaction, unlike full-length *KAR9*, was apparent in both wild-type and *bik1Δ* reporter strains, supporting a model in which Bik1p makes Kar9p accessible to Clb5p.

Clb5p Affects Kar9p Localization

The minimal Clb5p binding site that we have identified on Kar9p contains the serine 496 phosphorylation site identified by Liakopoulos *et al.* (2003). This suggests that Clb5p could affect the restriction of Kar9p to one SPB by promoting phosphorylation of this residue. Consistent with this idea, we observed that Kar9p-3GFP mislocalized to both SPBs in *clb5Δ* at a frequency that was similar to that seen in the *clb5Δbik1Δ* mutant. This was also similar to the mislocalization frequency observed in the *kar9-S496A* mutant, in which the phosphorylation of serine 496 is prohibited by replace-

ment of this residue with an alanine (Figure 7, A and B). Furthermore, the *kar9-S496A* mutation also eliminated the highest molecular weight band of Kar9p-tap normally seen in both asynchronous and hydroxyurea-arrested cells (Figure 7, C and D). Thus, the highest molecular weight band is dependent upon phosphorylation at serine 496.

DISCUSSION

Previously, two major functions were known for Bik1p on cMTs, stabilization of MT length and recruitment of dynein to MT plus ends. In this work, we present evidence that Bik1p has a novel role for Kar9p function. The interaction between Bik1p and Kar9p has at least two significant consequences. First, it alters the asymmetric localization of Kar9p at SPBs (Figure 3). *bik1Δ* mutants also display a SPB inheritance defect commensurate with the degree of Kar9p mislocalization at the new SPB, suggesting that not only is Kar9p required for proper SPB inheritance but also that its localization must be asymmetric. Second, in the absence of Bik1p, the phosphorylation of Kar9p is diminished, suggesting that Bik1p facilitates a phosphorylation event (Figure 5). These findings suggest a new mode of regulation in which a MT binding protein modulates the localization of another protein by facilitating changes in the phosphorylation status of that partner.

Although phosphorylation by other kinases is possible, two Cdc28p consensus sites have been identified in Kar9p at serines 197 and 496 (Liakopoulos *et al.*, 2003). The presence of a faint slower migrating band in the *kar9-S197A S496A* mutant and the presence of the highest molecular weight band in the S197A mutant supports the premise that at least one additional phosphorylation site exists in Kar9p (Figure 7C) (Maekawa and Schiebel 2004). The three bands of Kar9p that we observe are consistent with the highest band being phosphorylated at two sites, whereas the middle band represents phosphorylation at a single site. Thus, the lack of the highest molecular weight isoform in *bik1Δ* (Figure 5) suggests that Bik1p facilitates only one phosphorylation event. Furthermore, the absence of the highest molecular weight band in the *kar9-S496A* mutant in both asynchronous and hydroxyurea-treated cultures suggests that phosphorylation at serine 496 is required for the formation of the highest band.

We propose a model in which Bik1p promotes the phosphorylation of Kar9p by facilitating its interaction with Clb5p (Figure 6C). The Clb5p binding site on Kar9p contains serine 496 (Figure 6C), which is adjacent to the binding site of Bik1p (our unpublished data). Therefore, the binding of Bik1p could alter the conformation of Kar9p in such a way as to allow Clb5p-Cdc28p access to this site. We also cannot rule out the possibility that Bik1p could be protecting Kar9p from dephosphorylation, perhaps by limiting access to a phosphatase.

Several possibilities could account for the mechanism by which Bik1p promotes the asymmetric localization of Kar9p at one SPB. The asymmetry could be the result of just the interaction itself between Bik1p and Kar9p. However, this is unlikely because Bik1p-3GFP is localized to regions associated with both poles (Figure S2). Although it is also possible that the altered localization of Kar9p could affect its phosphorylation, we instead favor a model in which absence of Bik1p changes the phosphorylation of Kar9p, which in turn causes its aberrant localization. Consistent with this model, mutations in *cdc28* and several cyclins result in a similar alteration in the asymmetric localization of Kar9p (Liakopoulos *et al.*, 2003; Maekawa *et al.*, 2003; Maekawa

and Schiebel, 2004). It is also possible that the mislocalization of Kar9p might be indirect through an effect of the *bik1Δ* mutation on the localization of Bim1p, which also interacts with Kar9p. Distinguishing between these possibilities will require an analysis of *bik1* alleles that separate these activities.

It seems unlikely that the hypophosphorylation of Kar9p-tap in *bik1Δ* mutants is due to a cell cycle defect (in which a smaller proportion of *bik1Δ* cells are in S phase) for two reasons. First, the majority of cells in both wild type and *bik1Δ* are in S phase in the HU arrest and Kar9p is underphosphorylated in *bik1Δ* cells in comparison with wild type (Figure 5D). Second, *kip2Δ* mutants are expected to show a similar cell cycle profile as *bik1Δ* mutants. Kar9p-tap is more heavily phosphorylated in *kip2Δ* mutants than in *bik1Δ* mutants. In *kip2Δ* mutants, the Kar9p-tap isoforms were similar to those seen in wild type for both HU-arrested cells and asynchronous cells (Figure 5, B and D). Moreover, the cell cycle distribution of *bik1Δ* cells was not obviously different from that observed in *kip2Δ* or *dyn1Δ* when assayed by DAPI staining and bud size (our unpublished data).

Four MAPs and Kar9p

Before this work, three MAPs (Bim1p, Stu2p, and Kip2p) were known to interact with Kar9p (Korinek *et al.*, 2000; Lee *et al.*, 2000; Miller *et al.*, 2000; Maekawa *et al.*, 2003). The identification of Bik1p as a fourth MAP adds complexity to the model of how Kar9p associates with MTs. Our model shown in Figure 8 depicts Kar9p interacting with a successive series of MAPs. Bik1p interacts with Kar9p, changing its conformation. This facilitates the phosphorylation of Kar9p at serine 496 by Clb5p-Cdc28p, and this acts to restrict Kar9p to one SPB. Bim1p is involved in loading Kar9p onto the SPB (Liakopoulos *et al.*, 2003) and is responsible for tethering Kar9p to cMTs (Lee *et al.*, 2000; Korinek *et al.*, 2000; Miller *et al.*, 2000). The observation that Kar9p-3GFP fluorescence is less intense, but still present, at the tip of the MT in *kip2Δ* strains suggests that both Kip2p-dependent and -independent mechanisms are responsible for the localization of Kar9p at the plus end. In both *kip3Δ* and *bik1Δ kip3Δ* cells, we also observed that more cells displayed Kar9p-3GFP localization at plus ends and along the lengths of cMTs (Figure 2B). This could be due to either a possible direct interaction between Kar9p and Kip3p or to the increased stability of MTs in *kip3Δ*, allowing Kar9p to remain at the plus end.

Our model posits that the Bik1p-facilitated phosphorylation event occurs before the loading of Kar9p onto the SPB and its transit to the plus end. This phosphorylation of Kar9p is unlikely to be dependent upon its localization to MTs because Kar9p is phosphorylated in nocodazole-treated cells (Figure 5D). This suggests that Bik1p located at the SPB or in the cytoplasm, rather than Bik1p at the plus end, is contributing to Kar9p phosphorylation. Consistent with this, all three phospho-isoforms of Kar9p are present *bim1Δ* mutants, which display no Kar9p localization on MTs (Figure 5B).

Bik1p Has Functions in Both the Kar9p and Dynein Spindle Positioning Pathways

Deletion mutations between *KAR9* and *BIK1* are synthetically lethal with each other, suggesting that each protein carries out a vital function in one of the two partially redundant pathways. Whereas the placement of Bik1p in the dynein genetic pathway is explained by its recruitment of dynein to the cMT plus end (Sheeman *et al.*, 2003), our analyses here show that Bik1p also conducts a novel func-

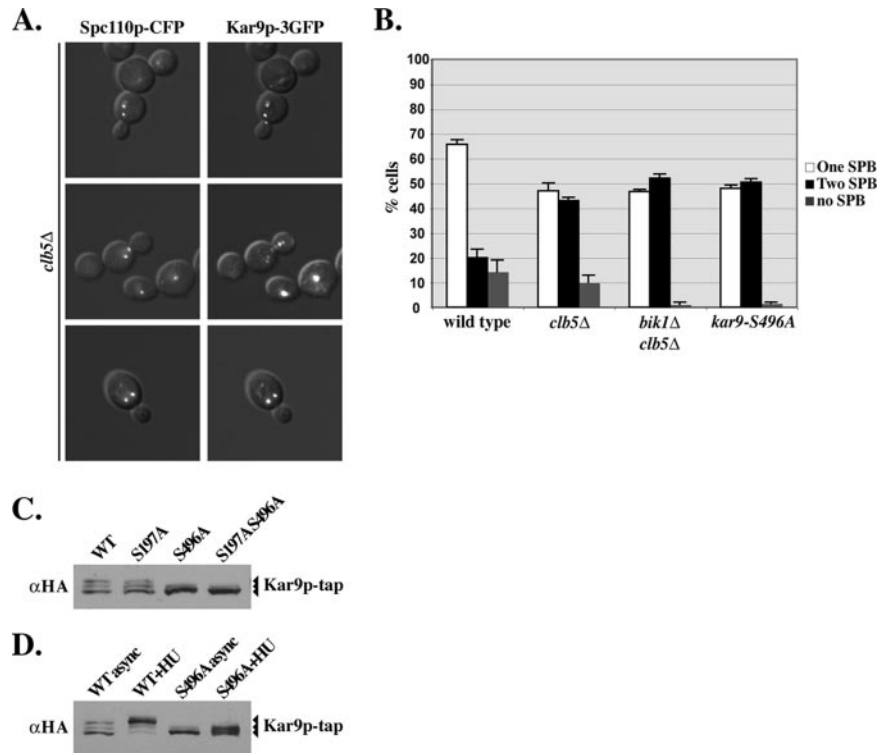
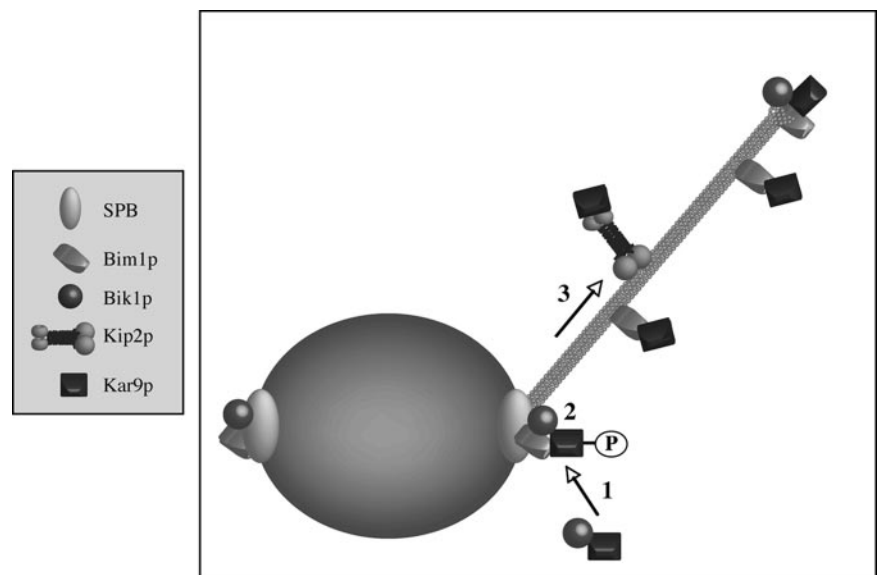


Figure 7. Bik1p, Clb5p, and serine 496 function in the restriction of Kar9p to one SPB. (A) Kar9p-3GFP was localized in *clb5Δ* strains containing SPBs labeled with Spc110p-CFP. Composites are shown of differential interference contrast with either GFP or CFP single images. (B) Quantification of Kar9p-3GFP at SPBs in wild-type (yRM4357; n = 201), *clb5Δ* (yRM5119; n = 200), and *bik1Δclb5Δ* (yRM5647; n = 251) cells with short bipolar spindles, and Kar9p-S496A-3GFP in the wild-type background (yRM6007; n = 250). Cells were grown in SC media – TRP at 30°C. Error bars denote the SEM of the counts in at least four separate experiments. (C) Extracts were prepared from asynchronous cultures of wild-type strains expressing *KAR9-tap* (yRM4366), *kar9-S197A-tap* (yRM6168), *kar9-S496A-tap* (yRM6015), and *kar9-S197A S496A-tap* (yRM6170). Cultures were grown to mid-exponential phase, lysed, and extracts were prepared for immunoblotting with α -HA. (D) Extracts were prepared from either asynchronous or hydroxyurea-arrested cultures expressing *KAR9-tap* (yRM4366) and *kar9-S496A-tap* (yRM6015).

tion in the Kar9p pathway. This function was not detected by genetic analysis (Miller and Rose, 1998). Although Bik1p and Kip2p act in both pathways, it is not surprising that these genes are not essential because Kar9p remains localized at the plus end in both mutants, albeit with a less intense fluorescence signal. Thus, one explanation for this apparent paradox is that residual amounts of Kar9p at the plus end are adequate for Kar9p to function effectively and link the plus ends of cMT to Myo2p, orienting the spindle. Nevertheless, the finding that Bik1p physically interacts with proteins of both the Kar9p and the dynein pathways provides new insight into how the two pathways may be coregulated.

Our data suggest that the role of Bik1p in SPB inheritance is to help restrict Kar9p localization to one SPB and thus one set of MTs. In this case, the incorrect inheritance of the new SPB should be proportional to the amount of Kar9p mislocalization at that SPB. In *bik1Δ*, we find that 70% of cells display Kar9p at both SPBs (Figure 3B). If spindle pole body inheritance were random in this 70%, then only half of the 70% (or 35% of the total cells) would be expected to display an SPB inheritance defect. Indeed, our findings show that 26% of *bik1Δ* cells do inherit the wrong pole (Figure 4). This is a more severe defect than is seen in other mutants of the dynein pathway, including *kip2Δ*. These data support the idea that the asymmetric localization of Kar9p to one SPB

Figure 8. A proposed mechanism for directing Kar9p to one SPB and MT plus end. In this model, Kar9p interacts with a succession of MAPs. 1) Bik1p-facilitated phosphorylation by Clb5p-Cdc28p restricts Kar9p to one SPB. 2) Bim1p loads Kar9p onto the SPB. 3) Bim1p tethers Kar9p to the MT and Kip2p transports a portion of Kar9p to the plus end. Clb4p also plays an important role in directing the localization of Kar9p (Liakopoulos *et al.* 2003; Maekawa *et al.* 2004).



and corresponding set of MTs designates that SPB as daughter bound. It further suggests that Bik1p acts in that designation. The involvement of Bik1p in the mechanism of SPB inheritance provides further insight into a mechanism for directing centrosomal inheritance during asymmetric cell division.

Kar9p shares a number of similarities with the adenomatous polyposis coli (APC) protein, its proposed functional homologue in higher eukaryotes (Bienz, 2001; reviewed in Näthke, 2004). Like Kar9p, APC is focused at the MT plus ends and binds EB1 (Su *et al.*, 1995; Mogensen *et al.*, 2002). The binding between APC and EB1 is thought to be regulated by phosphorylation by cyclin-dependent kinases. The target serine residue is conserved in yeast, serine 496 (Trzepacz *et al.*, 1997; Honnappa *et al.*, 2005). The Clb5p-binding domain of Kar9p encompasses this serine (Figure 6), supporting a conserved mechanism across species. Hence, it will be important to learn whether CLIP-170 proteins modulate the interactions of APC with microtubules or microtubule-organizing centers. Recently, APC and EB1 have been reported to localize to mammalian centrosomes, displaying a preferential localization to the older centrosome (Louie *et al.*, 2004). Thus, the generation of asymmetrical microtubule organizing centers seems to be a common paradigm in the mechanisms used to link a specific pole of the mitotic apparatus with cortical cues.

ACKNOWLEDGMENTS

We thank John Cooper, Fred Cross, Bruce Goode, David Pellman, Eric Phizicky, and the Yeast Resource Center for providing yeast strains, plasmids, and reagents. We thank Harold Hoops for critical reading of the manuscript. This work was supported by grants to R.K.M. from the Ruth Estrin Goldberg Memorial for Cancer Research, the Basil O'Connor Starter Scholar Research Award from the March of Dimes Birth Defects Foundation (#5-FY01-523), and the National Science Foundation (#MCB-0414768).

REFERENCES

Adames, N. R., and Cooper, J. A. (2000). Microtubule interactions with the cell cortex causing nuclear movements in *Saccharomyces cerevisiae*. *J. Cell Biol.* *149*, 863–874.

Beach, D. L., Thibodeaux, J., Maddox, P., Yeh, E., and Bloom, K. (2000). The role of the proteins Kar9 and Myo2 in orienting the mitotic spindle of budding yeast. *Curr. Biol.* *10*, 1497–1506.

Berlin, V., Styles, C. A., and Fink, G. R. (1990). *BIK1*, a protein required for microtubule function during mating and mitosis in *Saccharomyces cerevisiae*, colocalizes with tubulin. *J. Cell Biol.* *111*, 2573–2586.

Bienz, M. (2001). Spindles cotton on to junctions, APC and EB1. *Nat. Cell Biol.* *3*, E67–E68.

Byers, B., and Goetsch, L. (1975). Behavior of spindles and spindle plaques in the cell cycle and conjugation of *Saccharomyces cerevisiae*. *J. Bacteriol.* *124*, 511–523.

Carvalho, P., Gupta, M.L.J., Hoyt, M. A., and Pellman, D. (2004). Cell cycle control of kinesin-mediated transport of Bik1 (CLIP-170) regulates microtubule stability and dynein activation. *Dev. Cell* *6*, 815–829.

Cottingham, F. R., and Hoyt, M. A. (1997). Mitotic spindle positioning in *Saccharomyces cerevisiae* is accomplished by antagonistically acting microtubule motor proteins. *J. Cell Biol.* *138*, 1041–1053.

DeZwaan, T. M., Ellingson, E., Pellman, D., and Roof, D. M. (1997). Kinesin-related *KIP3* of *Saccharomyces cerevisiae* is required for a distinct step in nuclear migration. *J. Cell Biol.* *138*, 1023–1040.

Farkasovsky, M., and Kuntzel, H. (2001). Cortical Num1p interacts with the dynein intermediate chain Pac11 and cytoplasmic microtubules in budding yeast. *J. Cell Biol.* *152*, 251–262.

Heil-Chapdelaine, R. A., Oberle, J. R., and Cooper, J. A. (2000). The cortical protein Num1p is essential for dynein-dependent interactions of microtubules with the cortex. *J. Cell Biol.* *151*, 1337–1344.

Honnappa, S., John, C. M., Kostreva, D., Winkler, F. K., and Steinmetz, M. O. (2005). Structural insights into the EB1-APC interaction. *EMBO J.* *24*, 261–269.

Hwang, E. S., Kusch, J., Barral, Y., and Huffaker, T. C. (2003). Spindle orientation in *Saccharomyces cerevisiae* depends on the transport of microtubule ends along polarized actin cables. *J. Cell Biol.* *161*, 483–488.

Ito, T., Chiba, T., Ozawa, R., Yoshida, M., Hattori, M., and Sakaki, Y. (2001). A comprehensive two-hybrid analysis to explore the yeast protein interactome. *Proc. Natl. Acad. Sci. USA* *98*, 4569–4574.

James, P., Halladay, J., and Craig, E. A. (1996). Genomic libraries and a host strain designed for highly efficient two-hybrid selection in yeast. *Genetics* *144*, 1425–1436.

Kahana, J. A., Schnapp, B. J., and Silver, P. A. (1995). Kinetics of spindle pole body separation in budding yeast. *Proc. Natl. Acad. Sci. USA* *92*, 9707–9711.

Korinek, W. S., Copeland, M. J., Chaudhuri, A., and Chant, J. (2000). Molecular linkage underlying microtubule orientation toward cortical sites in yeast. *Science* *287*, 2257–2259.

Kosco, K. A., Pearson, C. G., Maddox, P. S., Wang, P. J., Adams, I. R., Salmon, E. D., Bloom, K., and Huffaker, T. C. (2001). Control of microtubule dynamics by Stu2p is essential for spindle orientation and metaphase chromosome alignment in yeast. *Mol. Biol. Cell.* *12*, 2870–2880.

Kusch, J., Meyer, A., Snyder, M. P., and Barral, Y. (2002). Microtubule capture by the cleavage apparatus is required for proper spindle positioning in yeast. *Genes Dev.* *16*, 1627–1639.

Lee, L., Tirnauer, J. S., Li, J., Schuyler, S. C., Liu, J. Y., and Pellman, D. (2000). Positioning of the mitotic spindle by a cortical-microtubule capture mechanism. *Science* *287*, 2260–2262.

Lee, W.-L., Oberle, J. R., and Cooper, J. A. (2003). The role of the lissencephaly protein Pac1 during nuclear migration in budding yeast. *J. Cell Biol.* *160*, 355–364.

Liakopoulos, D., Kusch, J., Grava, S., Vogel, J., and Barral, Y. (2003). Asymmetric loading of Kar9 onto spindle poles and microtubules ensures proper spindle alignment. *Cell* *112*, 561–574.

Lin, H., de Carvalho, P., Kho, D., Tai, C. Y., Pierre, P., Fink, G. R., and Pellman, D. (2001). Polyploids require Bik1 for kinetochore-microtubule attachment. *J. Cell Biol.* *155*, 1173–1184.

Loog, M., and Morgan, D. O. (2005). Cyclin specificity in the phosphorylation of cyclin-dependent kinase substrates. *Nature* *434*, 104–108.

Louie, R. K., Bahmanyar, S., Siemers, K. A., Votin, V., Chang, P., Stearns, T., Nelson, W. J., Barth, A. I. (2004). Adenomatous polyposis coli and EB1 localize in close proximity of the mother centriole and EB1 is a functional component of centrosomes. *J. Cell Sci.* *117*, 1117–1128.

Maekawa, H., and Schiebel, E. (2004). Cdk1-Clb4 controls the interaction of astral microtubule plus ends with subdomains of the daughter cell cortex. *Genes Dev.* *18*, 1709–1724.

Maekawa, H., Usui, T., Knop, M., and Schiebel, E. (2003). Yeast Cdk1 translocates to the plus end of cytoplasmic microtubules to regulate bud cortex interactions. *EMBO J.* *22*, 438–449.

Miller, R. K. (2004). Monitoring spindle assembly and disassembly in yeast by indirect immunofluorescence. In: *Cell Cycle Checkpoint Control Protocols*, ed. H. B. Lieberman, Totowa, NJ: Humana Press. *Methods Mol. Biol.* *241*, 341–352.

Miller, R. K., Cheng, S.-C., and Rose, M. D. (2000). Bim1p/Yeb1p mediates the Kar9p-dependent cortical attachment of cytoplasmic microtubules. *Mol. Biol. Cell* *11*, 2949–2959.

Miller, R. K., Heller, K. K., Frisen, L., Wallack, D. L., Loayza, D., Gammie, A. E., and Rose, M. D. (1998). The kinesin-related proteins, Kip2p and Kip3p, function differently in nuclear migration in yeast. *Mol. Biol. Cell* *9*, 2051–2068.

Miller, R. K., Matheos, D., and Rose, M. D. (1999). The cortical localization of the microtubule orientation protein, Kar9p, is dependent upon actin and proteins required for polarization. *J. Cell Biol.* *144*, 963–975.

Miller, R. K., and Rose, M. D. (1998). Kar9p is a novel cortical protein required for cytoplasmic microtubule orientation in yeast. *J. Cell Biol.* *140*, 377–390.

Mogensen, M., Tucker, J. B., Mackie, J. B., Prescott, A. R., and Näthke, I. S. (2002). The adenomatous polyposis coli protein unambiguously localizes to microtubule plus ends and is involved in establishing parallel arrays of microtubule bundles in highly polarized epithelial cells. *J. Cell Biol.* *157*, 1041–1048.

Muhua, L., Karpova, T. S., and Cooper, J. A. (1994). A yeast actin-related protein homologous to that in vertebrate dynactin complex is important for spindle orientation and nuclear migration. *Cell* *78*, 669–679.

Näthke, I. S. (2004). The adenomatous polyposis coli protein: the Achilles heel of the gut epithelium. *Annu. Rev. Cell Dev. Biol.* *20*, 337–366.

- Pereira, G., Tanaka, T. U., Nasmyth, K., and Schiebel, E. (2001). Modes of spindle pole body inheritance and segregation of the Bfa1p-Bub2p checkpoint protein complex. *EMBO J.* *20*, 6359–6370.
- Puig, O., Caspary, F., Rigaut, G., Rutz, B., Bouveret, E., Bragado-Nilsson, E., Wilm, M., and Seraphin, B. (2001). The tandem affinity purification (TAP) method: a general procedure of protein complex purification. *Methods* *24*, 218–229.
- Schuyler, S. C., and Pellman, D. (2001). Microtubule “plus-end-tracking proteins”: the end is just the beginning. *Cell* *105*, 421–424.
- Segal, M., Bloom, K., and Reed, S. I. (2000a). Bud6 directs sequential microtubule interactions with the bud tip and bud neck during spindle morphogenesis in *Saccharomyces cerevisiae*. *Mol. Biol. Cell* *11*, 3689–3702.
- Segal, M., Clarke, D. J., Maddox, P., Salmon, E. D., Bloom, K., and Reed, S. I. (2000b). Coordinated spindle assembly and orientation requires Clb5p-dependent kinase in budding yeast. *J. Cell Biol.* *148*, 441–452.
- Segal, M., Clarke, D. J., and Reed, S. I. (1998). Clb5-associated kinase activity is required early in the spindle pathway for correct preanaphase nuclear positioning in *Saccharomyces cerevisiae*. *J. Cell Biol.* *143*, 135–145.
- Sheeman, B., Carvalho, P., Sagot, I., Geiser, J., Kho, D., Hoyt, M. A., and Pellman, D. (2003). Determinants of *S. cerevisiae* dynein localization and activation: implications for the mechanism of spindle positioning. *Curr. Biol.* *13*, 364–372.
- Su, L. K., Burrell, M., Hill, D. E., Gyuris, J., Brent, R., Wiltshire, R., Trent, J., Vogelstein, B., and Kinzler, K. W. (1995). APC binds to the novel protein EB1. *Cancer Res.* *55*, 2972–2977.
- Sullivan, D. S., and Huffaker, T. C. (1992). Astral microtubules are not required for anaphase B in *Saccharomyces cerevisiae*. *J. Cell Biol.* *119*, 379–388.
- Theesfeld, C. L., Irazoqui, J. E., Bloom, K., and Lew, D. J. (1999). The role of actin in spindle orientation changes during the *Saccharomyces cerevisiae* cell cycle. *J. Cell Biol.* *146*, 1019–1032.
- Trzepacz, C., Lowy, A. M., Kordich, J. J., and Groden, J. (1997). Phosphorylation of the tumor suppressor adenomatous polyposis coli (APC) by the cyclin-dependent kinase p34^{cd2}. *J. Biol. Chem.* *272*, 21681–21684.
- Yeh, E., Skibbens, R. V., Cheng, J. W., Salmon, E. D., and Bloom, K. (1995). Spindle dynamics and cell cycle regulation of dynein in the budding yeast, *Saccharomyces cerevisiae*. *J. Cell Biol.* *130*, 687–700.
- Yeh, E., Yang, C., Chin, E., Maddox, P., Salmon, E. D., Lew, D. J., and Bloom, K. (2000). Dynamic positioning of mitotic spindles in yeast: role of microtubule motors and cortical determinants. *Mol. Biol. Cell* *11*, 3949–3961.
- Yin, H., Pruyn, D., Huffaker, T. C., and Bretscher, A. (2000). Myosin V orientates the mitotic spindle in yeast. *Nature* *406*, 1013–1015.
- Yoder, T. J., Pearson, C. G., Bloom, K., and Davis, T. N. (2003). The *Saccharomyces cerevisiae* spindle pole body is a dynamic structure. *Mol. Biol. Cell.* *14*, 3494–3505.